Walther Meißner Institut

BAdW | BAYERISCHE AKADEMIE DER WISSENSCHAFTEN

Technische Universität München

Superconductivity and Low Temperature Physics I

Lecture Notes
Winter Semester 2021/2022

R. Gross

Chapter 6

Flux Pinning and Critical Currents

Walther Meißner Institut

BAdW BAYERISCHE AKADEMIE DER WISSENSCHAFTEN

Technische Universität München

Superconductivity and Low Temperature Physics I

Lecture No. 11

R. Gross

6 Flux Pinning and Critical Currents

6.1 Power Applications of Superconductivity

- power applications require high T_c, B_{c2}, **and J_c**

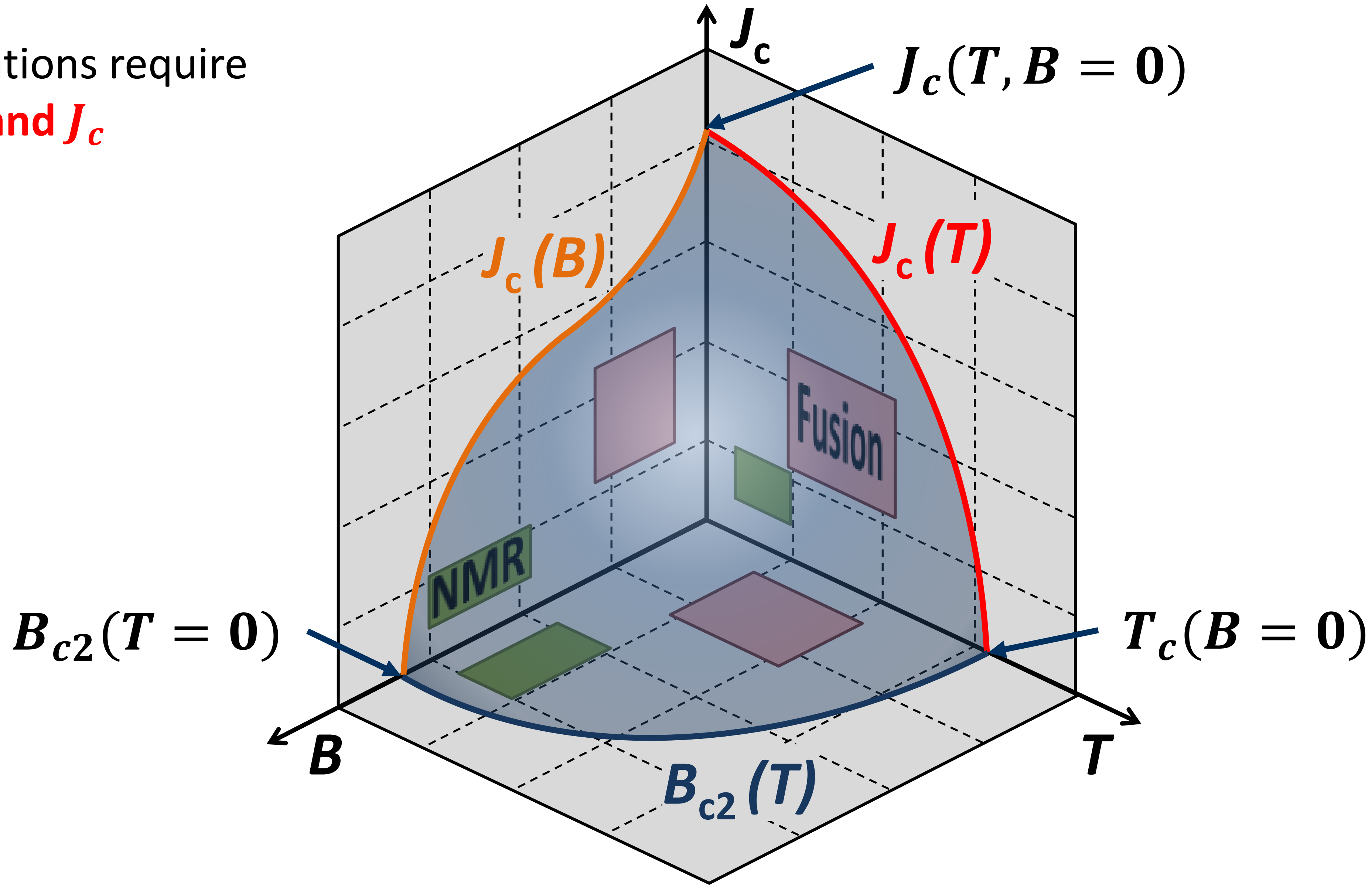

6.1.1 Examples

- ***energy transport and storage***

fault current limiter

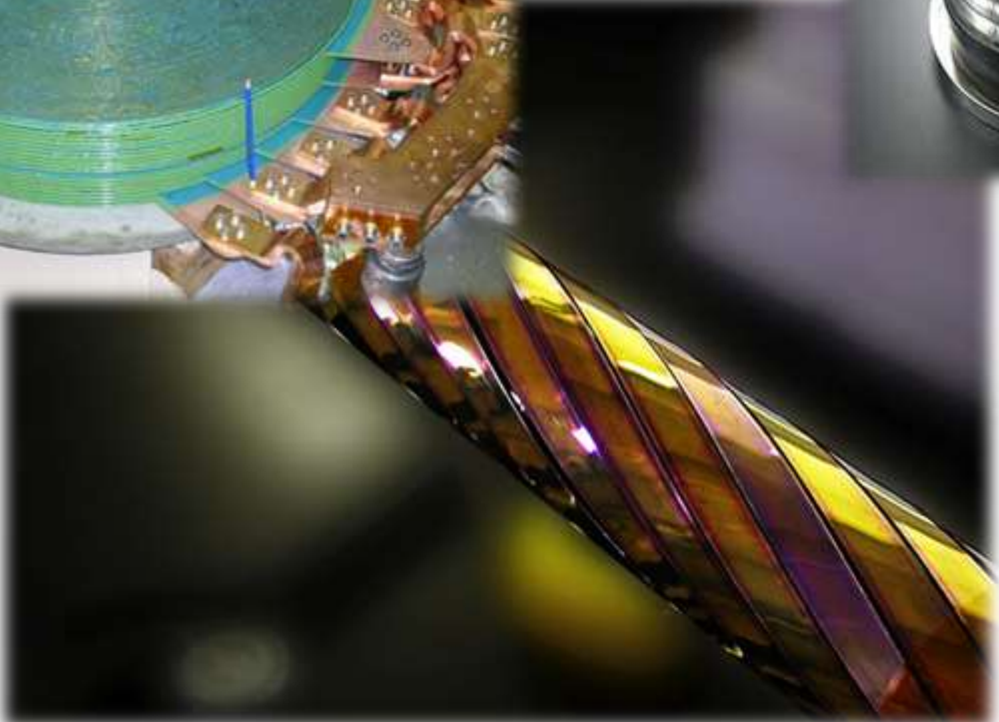

SMES (2 MJ)
superconducting magnetic energy storage

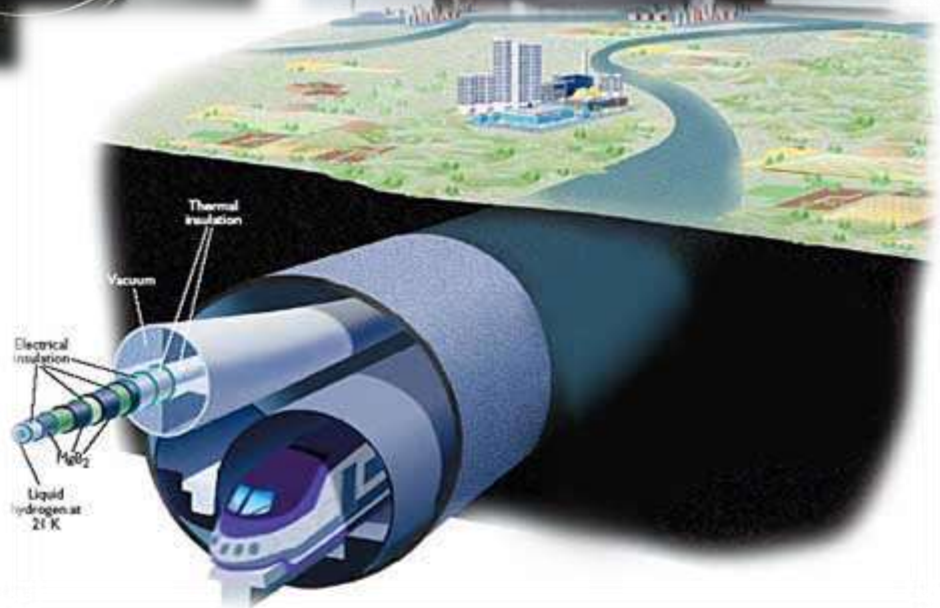

6.1.1 Examples

- ***fault current limiter***

Nexans fault current limiter delivered on site in Essen

the fault current limiter for AmpaCity is designed to limit a 38 kA peak short circuit current to about 10 kA.

6.1.1 Examples

Comparison of the amount of space consumed by a superconducting cable (blue) with copper wires carrying the same amount of current

6.1 Power Applications of Superconductivity

6.1.1 Examples

- *superconducting magnets*

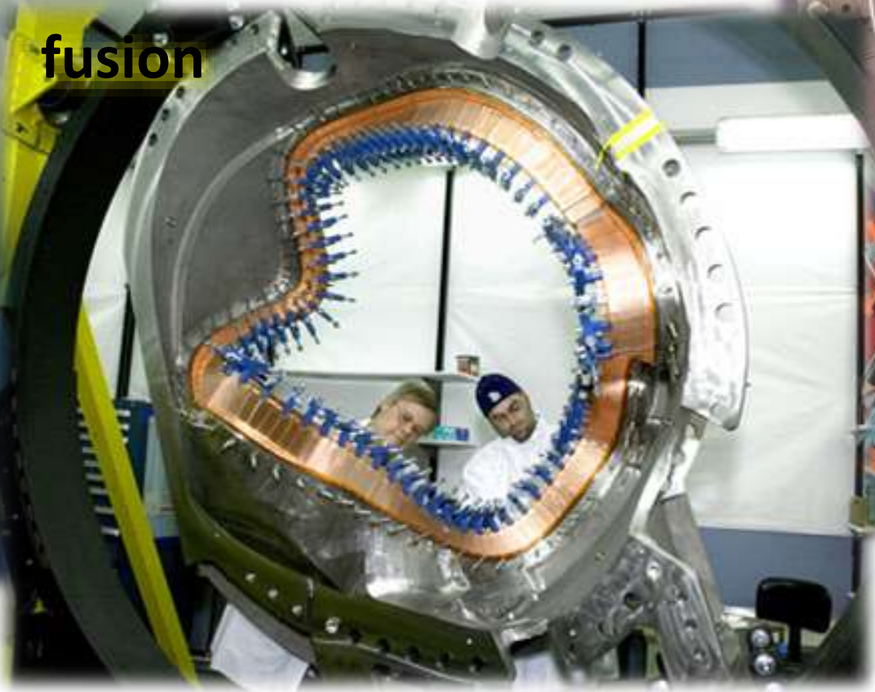

6.1.1 Examples

45-T Hybrid Magnet

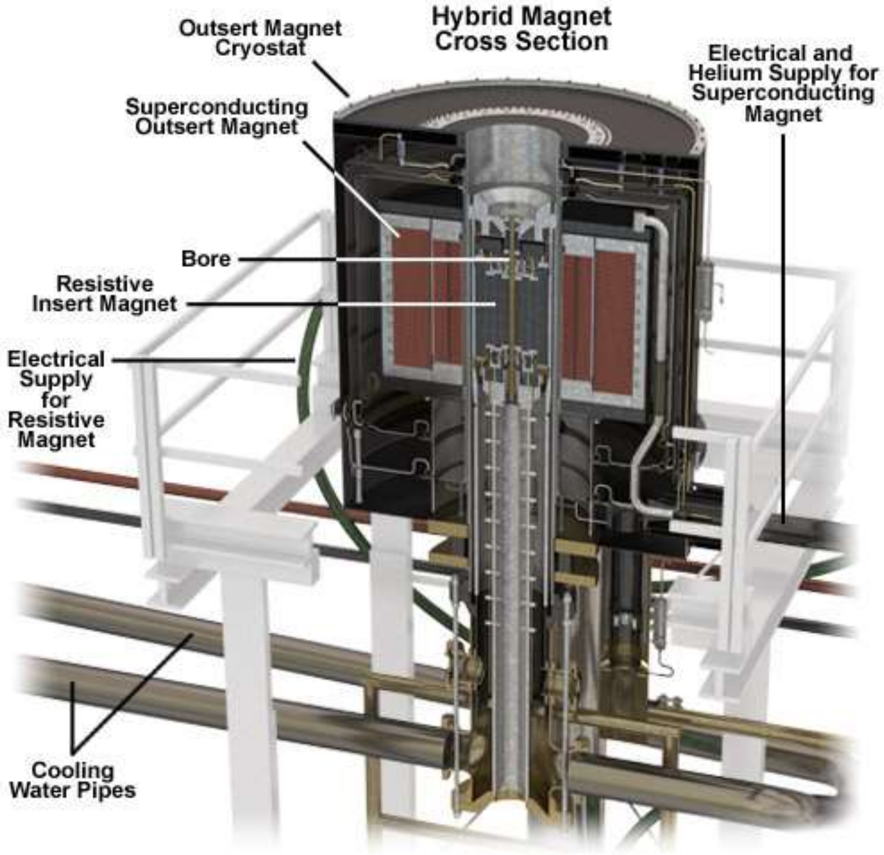

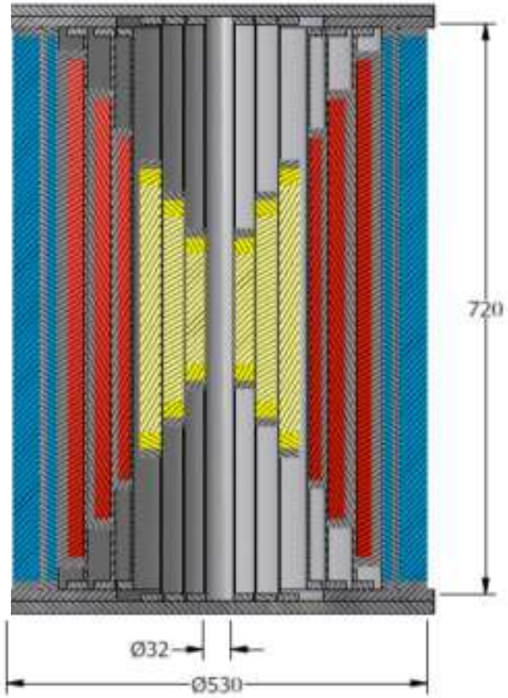

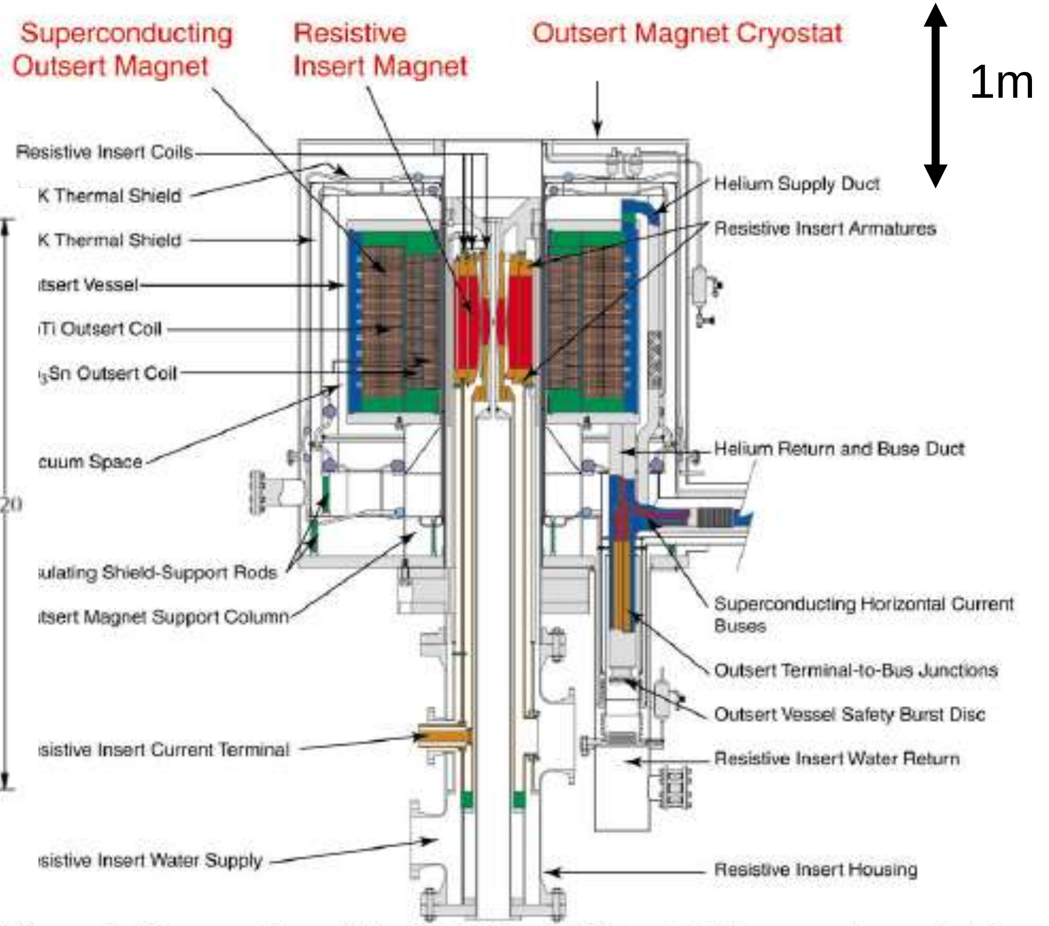

Figure 1 – Cross section of the 45-T Hybrid Magnet. The magnet cryostat is about 8 feet in diameter and the large-diameter part is about 9 feet tall.

NATIONAL HIGH MAGNETIC FIELD LAB

45 Tesla, 32 mm Bore Hybrid Magnet

6.1.1 Examples

AMS-02 is the **Alpha Magnetic Spectrometer**, a superconducting particle physics experiment which will be launched on the Space Shuttle and installed on the International Space Station. The project is an international collaboration of 56 research institutes from 16 countries.

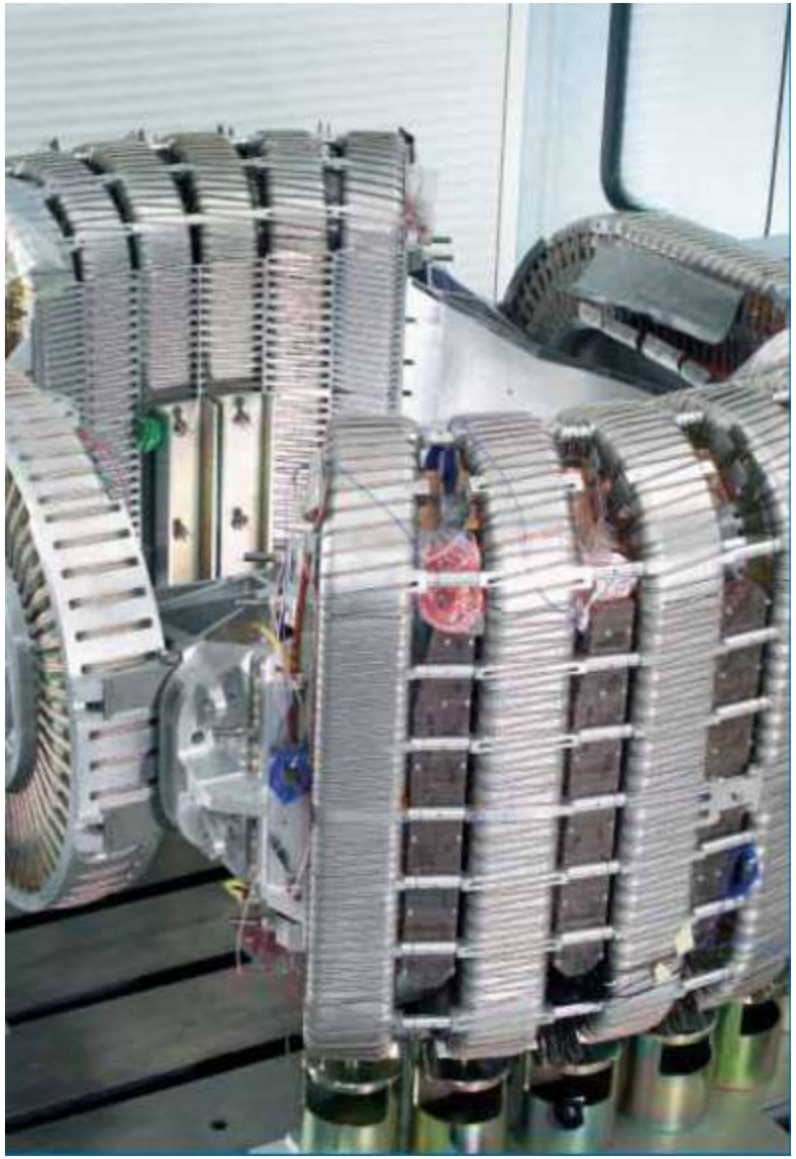

Central Magnetic Field $B_x(0,0)$	0.86 T
Dipole Bending Power	0.78 Tm²
Room Temperature Bore Diameter	1100 mm
Cryostat Outside Diameter	2800 mm
Overall Cryostat Height	1500 mm
Cold Mass	2200 kg
Operating Temperature	1.8 K
Superfluid Helium Capacity	2500 litre
Maximum Stray Field at R=2.3m	15.2 mT
Maximum Stray Field at Y=2.3m	7.6 mT
Maximum Stray Field at R=3.0m	3.9 mT
Peak Field on the Dipole Coils	6.59 T
Peak Field on the Racetrack Coils	5.91 T
Magnetic Torque (in Earths Field)	0.27 Nm
Nominal Operating Magnet Current	459 A
Stored Energy	5.15 MJ
Nominal Magnet Inductance	48.9 H

http://www.scientificmagnetics.co.uk/special-superconducting-magnets.htm

6.1.1 Examples

High Field Magnets for NMR

1.02 GHz(24 T) NMR magnet (world record at 2015)
DI-BSCCO Type HT-CA/Insert coil (3.6 T)

6.1.1 Examples

High Field Magnets for NMR

Bavarian NMR Center (BNMRZ)

AV Neo 1200 ("Charlie")

Magnet:

1200 MHz (1H), Bruker Karlsruhe 2022, pumped (2 K)

Console:

Bruker Avance III HD, channels: 1H, X, Y, Z

Workstation:

PC (Linux)

Probes:

3 mm cryo-TCI (1H, 13C, 15N) with z-gradient

TXI (1H, 13C, 15N) with z-gradient

MAS probes (not yet installed)

6.1.2 Materials Requirements

- high T_c, B_{c2}, J_c

- manufacturability
- low cost
- availability (sustainability)

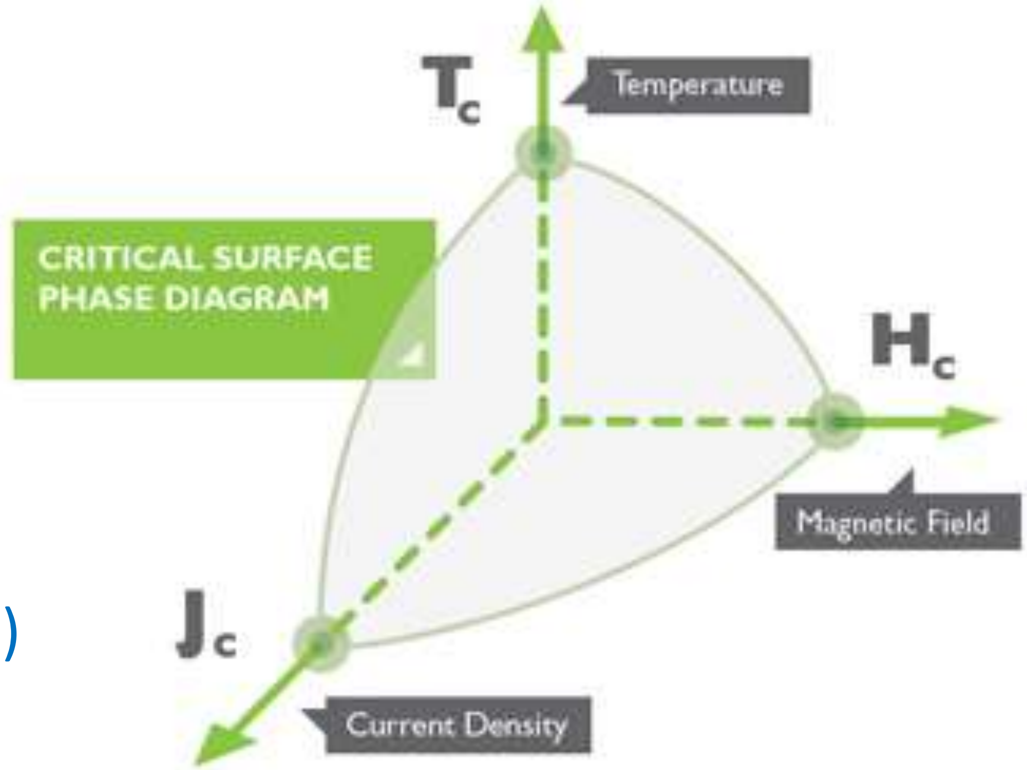

6.1.2 Materials Requirements

material parameters:

- important low T_c superconductors (application in commercial magnets)

	NbTi	Nb_3Sn
material:	1:1 alloy	intermetallic compound
T_c	9.6 K	18 K
$B_{c2}(T=0)$	10.5 - 15 T	23 - 29 T

- high T_c superconductors

	BSCCO	YBCO
material:	powder in Ag-tube	thin film on metal tape
T_c	110 K	91 K
$B_{c2}(T = 0)$	$\sim$ 1000 T	800 T

still under development

material parameters of type-II superconductors

Material	Transition Temperature (K)	Upper Critical Field (T)
NbTi	10	15
PbMoS	14.4	6.0
V_3Ga	14.8	2.1
NbN	15.7	1.5
V_3Si	16.9	2.35
Nb_3Sn	18.0	24.5
Nb_3Al	18.7	32.4
$Nb_3(AlGe)$	20.7	44
Nb_3Ge	23.2	38

Blatt, Frank J., Modern Physics, McGraw-Hill, 1992

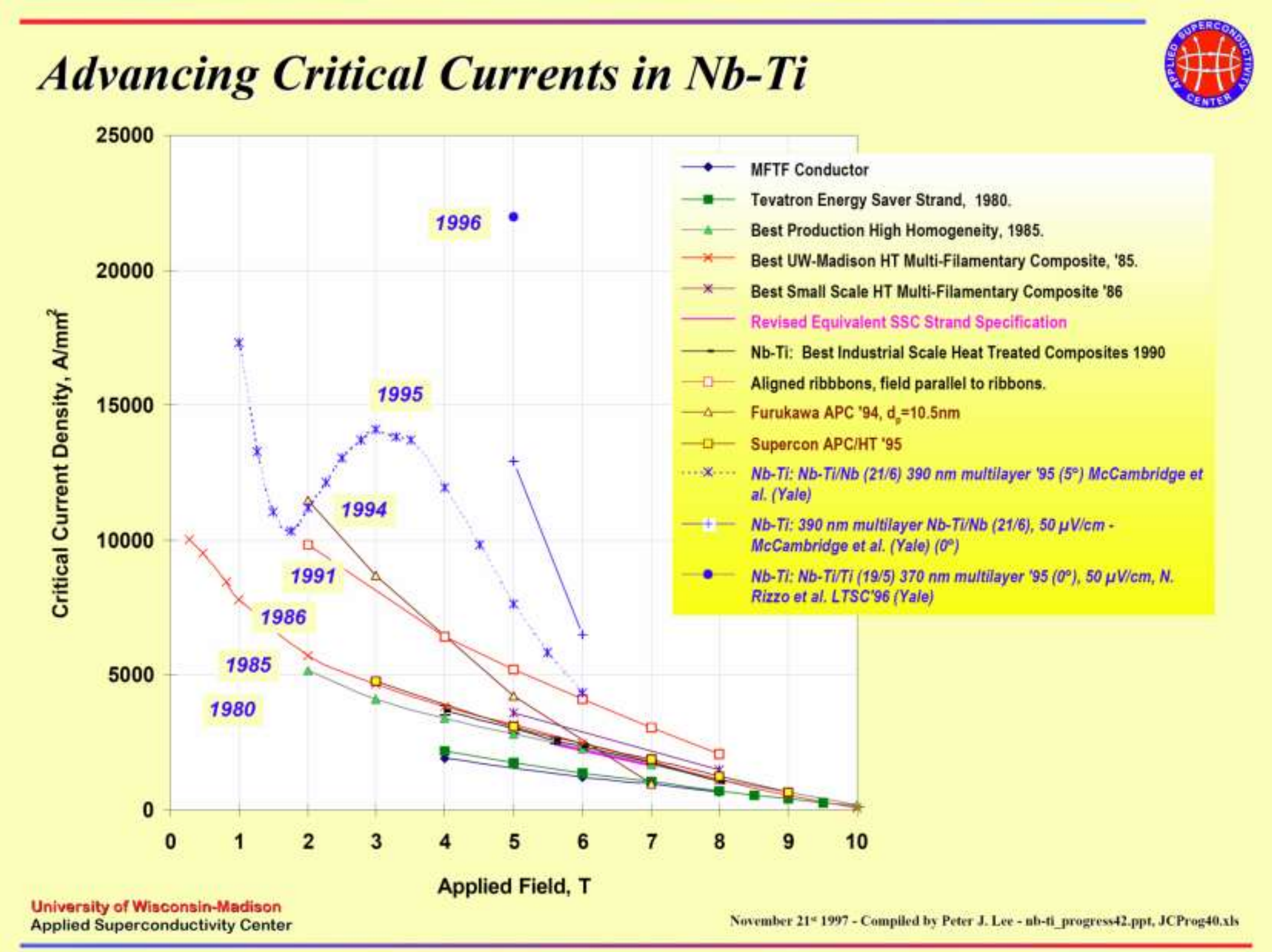

improvement of critical current density of superconductors requires decades of materials engineering

1997

https://nationalmaglab.org/

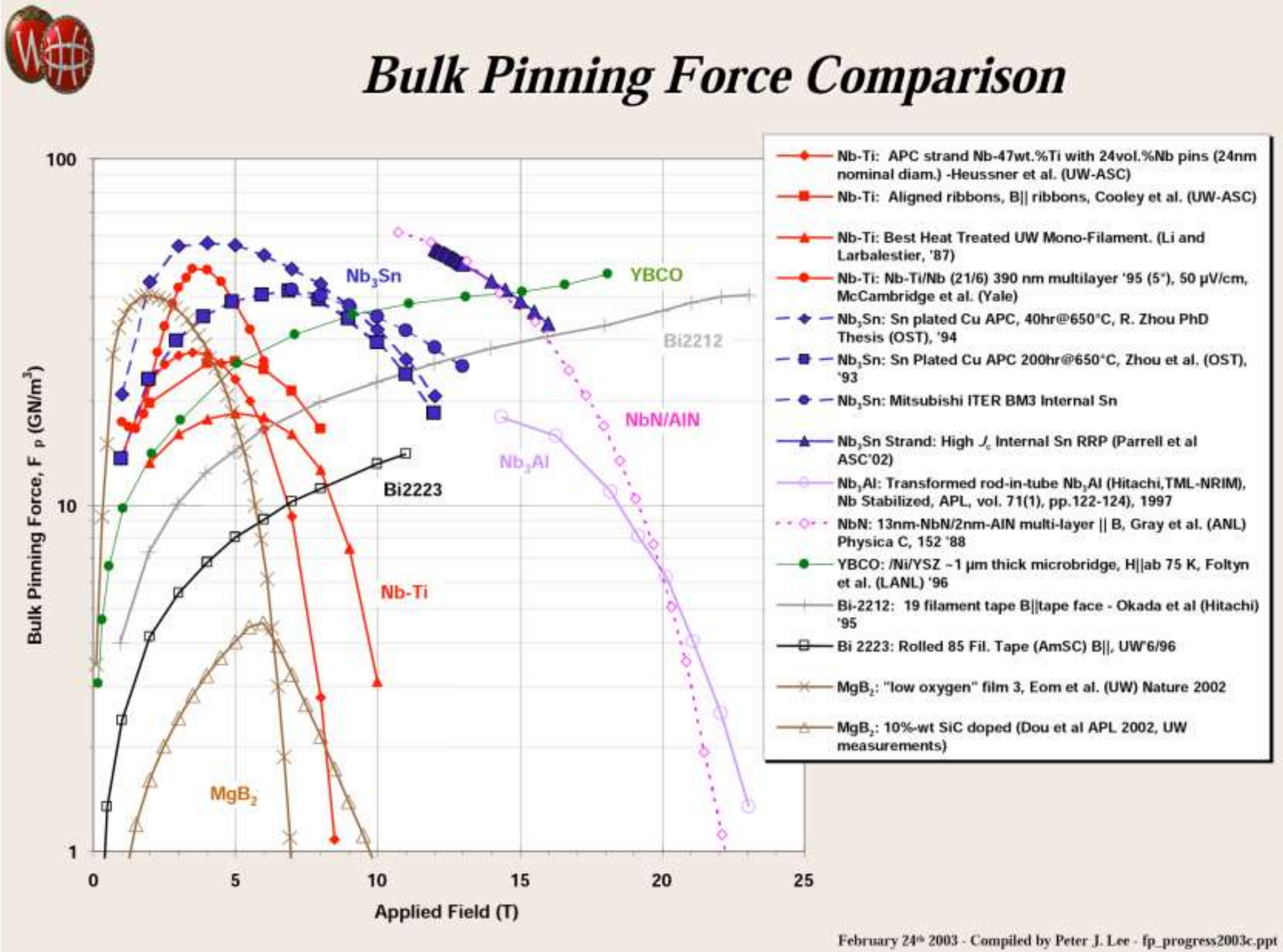

improvement of pinning force by defect engineering

2003

https://nationalmaglab.org/

6.1.2 Materials Requirements

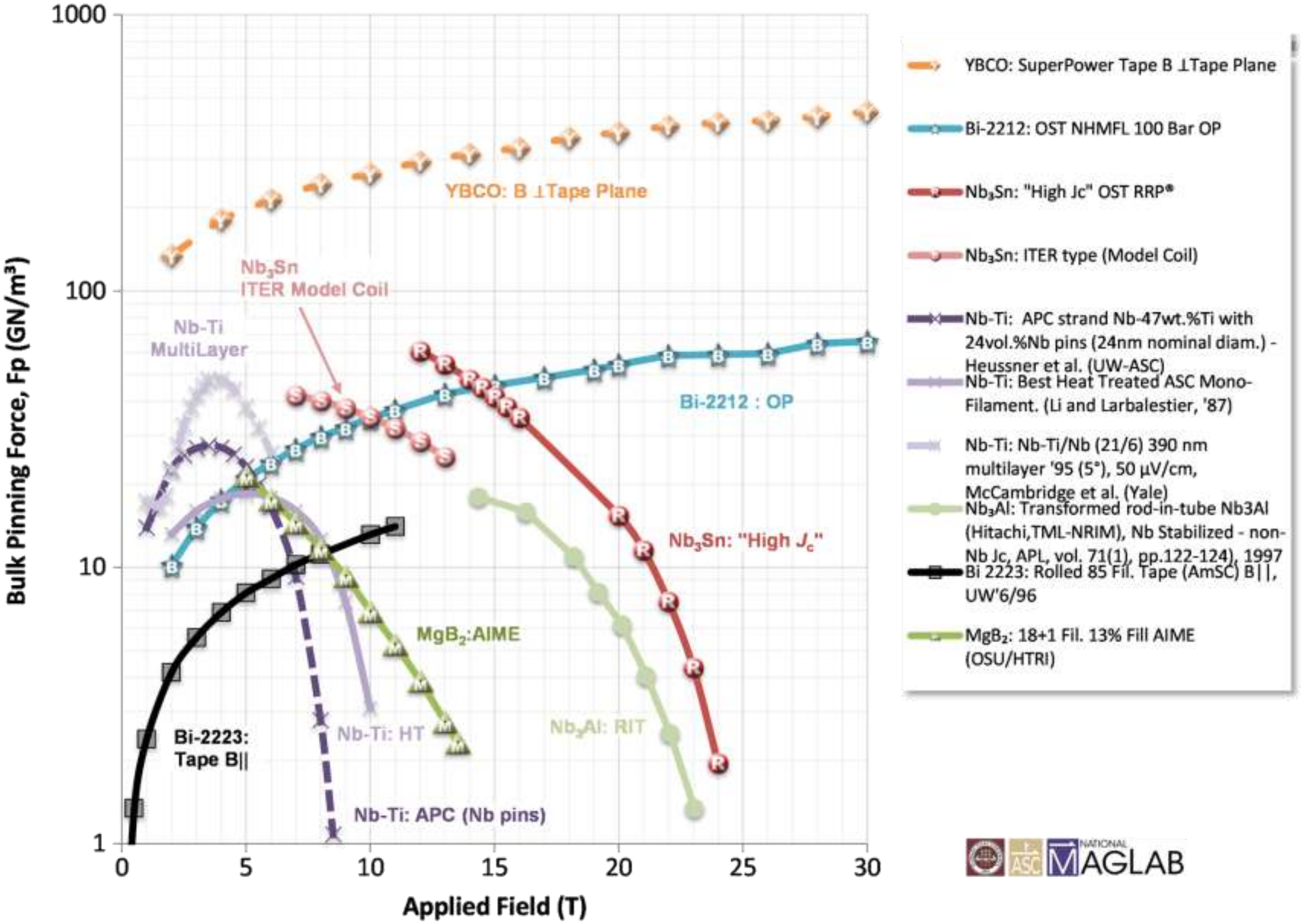

improvement of pinning force by defect engineering

2018

https://nationalmaglab.org/

6.1.2 Materials Requirements

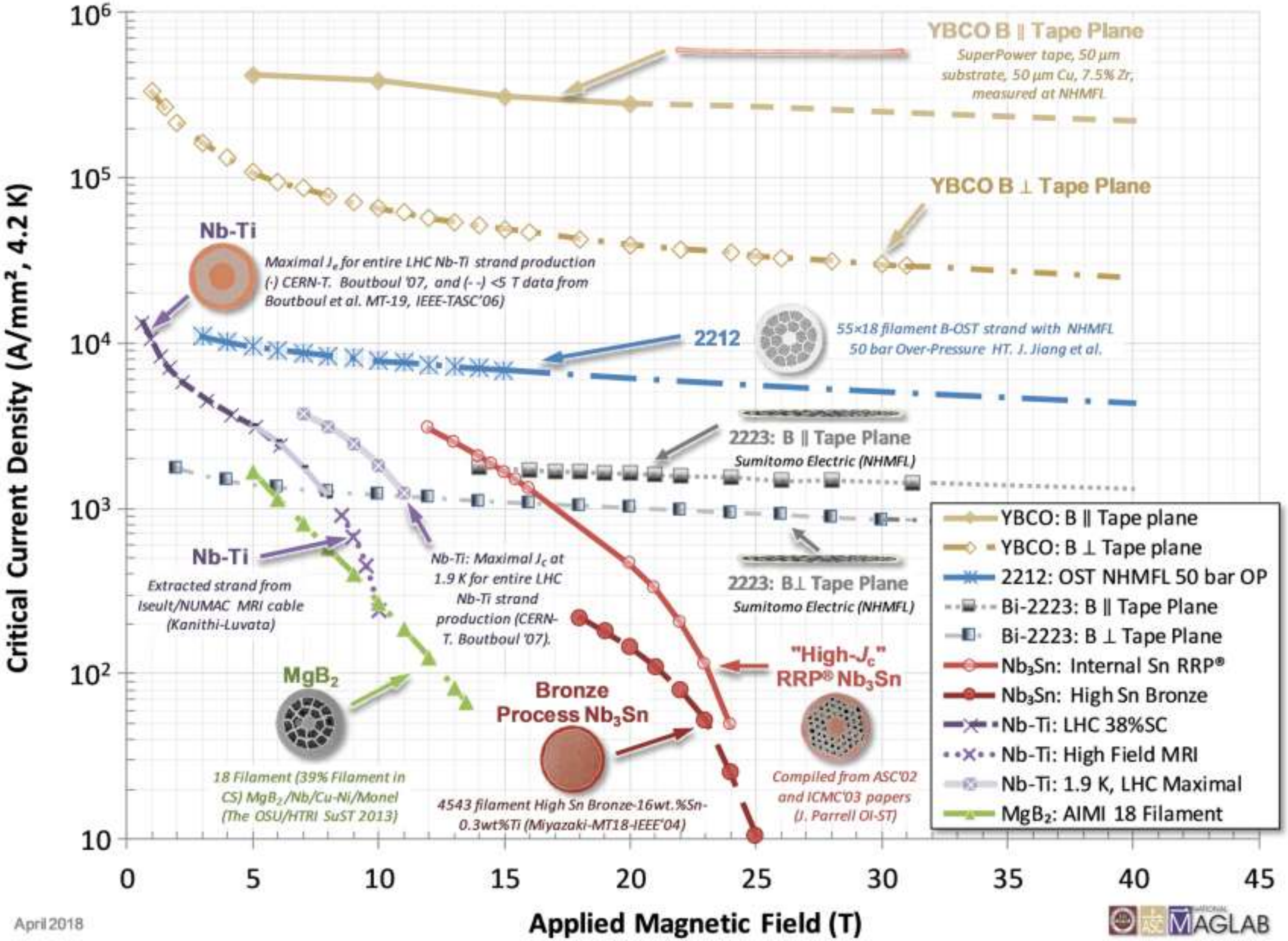

Non-stabilizer Critical Current Density vs. Applied Field for Superconductors Available in Long Lengths

April 16, 2018

2018

https://nationalmaglab.org/

References (updated 4/2021)

- YBCO: Tape, ∥ Tape-plane, SuperPower. REBCO: SP26 tape, 50 µm substrate, 7.5%Zr. Measured at NHMFL by Valeria Braccini, Jan Jaroszynski and Aixia Xu: DOI: 10.1088/0953-2048/24/3/035001
- YBCO: Tape, ⊥ Tape-plane. REBCO: SP26 tape, 50 µm substrate, 7.5%Zr. Measured at NHMFL by Valeria Braccini, Jan Jaroszynski and Aixia Xu: DOI: 10.1088/0953-2048/24/3/035001
- Bi-2223: B ∥ Tape plane: Sumitomo Electric Industries. Measured at NHMFL (D. Abraimov) unpublished
- Bi-2223 (Carrier Controlled): B ⊥ Tape-plane "DI" BSCCO "Carrier Controlled" Sumitomo Electric Industries (MEM'13 presented by Kazuhiko Hayashi).
- Bi-2223 (2012 production): B ⊥ Tape-plane "DI" BSCCO (measured at NHMFL by Jianyi Jiang and Dmytro Abraimov Oct. 2013).
- 2212: OST NHMFL 50 bar overpressure HT. Sample pmm170123, 0.78 mm Diam. (after HT) , OST 55x18 composite using nGimat powder. Jiang J, Bradford G, Hossain SI, Brown MD, Cooper J, Miller E, Huang Y, Miao H, Parrell JA, White M, Hunt A, Sengupta S, Revur R, Shen T, Kametani F, Trociewitz UP, Hellstrom EE, Larbalestier DC (2019) High-Performance Bi-2212 Round Wires Made With Recent Powders. IEEE Transactions on Applied Superconductivity, 29(5):1–5. DOI: 10.1109/TASC.2019.2895197
- Nb-47Ti: 0-6 T - Boutboul et al. MT-19: Boutboul, T.; Le Naour, S.; Leroy, D.; Oberli, L.; Previtali, V.; , "Critical Current Density in Superconducting Nb-Ti Strands in the 100 mT to 11 T Applied Field Range," Applied Superconductivity, IEEE Transactions on , vol.16, no.2, pp.1184-1187, June 2006. DOI: 10.1109/TASC.2006.870777
- Nb-47Ti 1.8 K 5-8 T Maximal for whole LHC NbTi strand production (CERN-T. Boutboul '07)
- Nb-47Ti 4.2 K for the LHC insertion quadrupole strand (T. Boutboul, S. Le Naour, D. Leroy, L. Oberli, and V. Previtali, “Critical Current Density in Superconducting Strands in the 100 mT to 11 T Applied Field Range,” IEEE Transactions on Applied Superconductivity, vol. 16, no. 2, pp. 1184–1187, Jun. 2006 DOI: 10.1109/TASC.2006.870777)
- Nb-47Ti 4.22 K for 11.75 T Iseult/INUMAC MRI: Kanithi H, Blasiak D, Lajewski J, Berriaud C, Vedrine P and Gilgrass G 2014 Production Results of 11.75 Tesla Iseult/INUMAC MRI Conductor at Luvata IEEE Transactions on Applied Superconductivity 24 1–4 DOI: 10.1109/TASC.2013.2281417
- Nb_3Sn (RRP®): Non-Cu Jc Internal Sn OI-ST RRP® 1.3 mm, Parrell, J.A.; Youzhu Zhang; Field, M.B.; Cisek, P.; Seung Hong; "High field Nb_3Sn conductor development at Oxford Superconducting Technology," Applied Superconductivity, IEEE Transactions on , vol.13, no.2, pp. 3470- 3473, June 2003.
- DOI: 10.1109/TASC.2003.812360 and Nb_3Sn Conductor Development for Fusion and Particle Accelerator Applications J. A. Parrell, M. B. Field, Y. Zhang, and S. Hong, AIP Conf. Proc. 711, 369 (2004), DOI: 10.1063/1.1774590.
- Nb_3Sn (High Sn Bronze): T. Miyazaki et al. MT18 - fig3, Miyazaki, T.; Kato, H.; Hase, T.; Hamada, M.; Murakami, Y.; Itoh, K.; Kiyoshi, T.; Wada, H.; , "Development of high Sn content bronze processed Nb3Sn superconducting wire for high field magnets," Applied Superconductivity, IEEE Transactions on , vol.14, no.2, pp. 975- 978, June 2004, DOI: 10.1109/TASC.2004.830344
- MgB_2: 18 Filament - The OSU/HTRI C 2 mol% AIMI ("Advanced Internal Mg Infiltration") 33.8 Filament to strand ratio, 39.1% MgB_2 in filament. (DOI: 10.1088/0953-2048/25/11/115023)
- G. Z. Li, M. D. Sumption, J. B. Zwayer, M. A. Susner, M. A. Rindfleisch, C. J. Thong, M. J. Tomsic, and E. W. Collings, “Effects of carbon concentration and filament number on advanced internal Mg infiltration-processed MgB_2 strands,” Superconductor Science and Technology, vol. 26, no. 9, p. 095007, Sep. 2013.

6.1.2 Materials Requirements

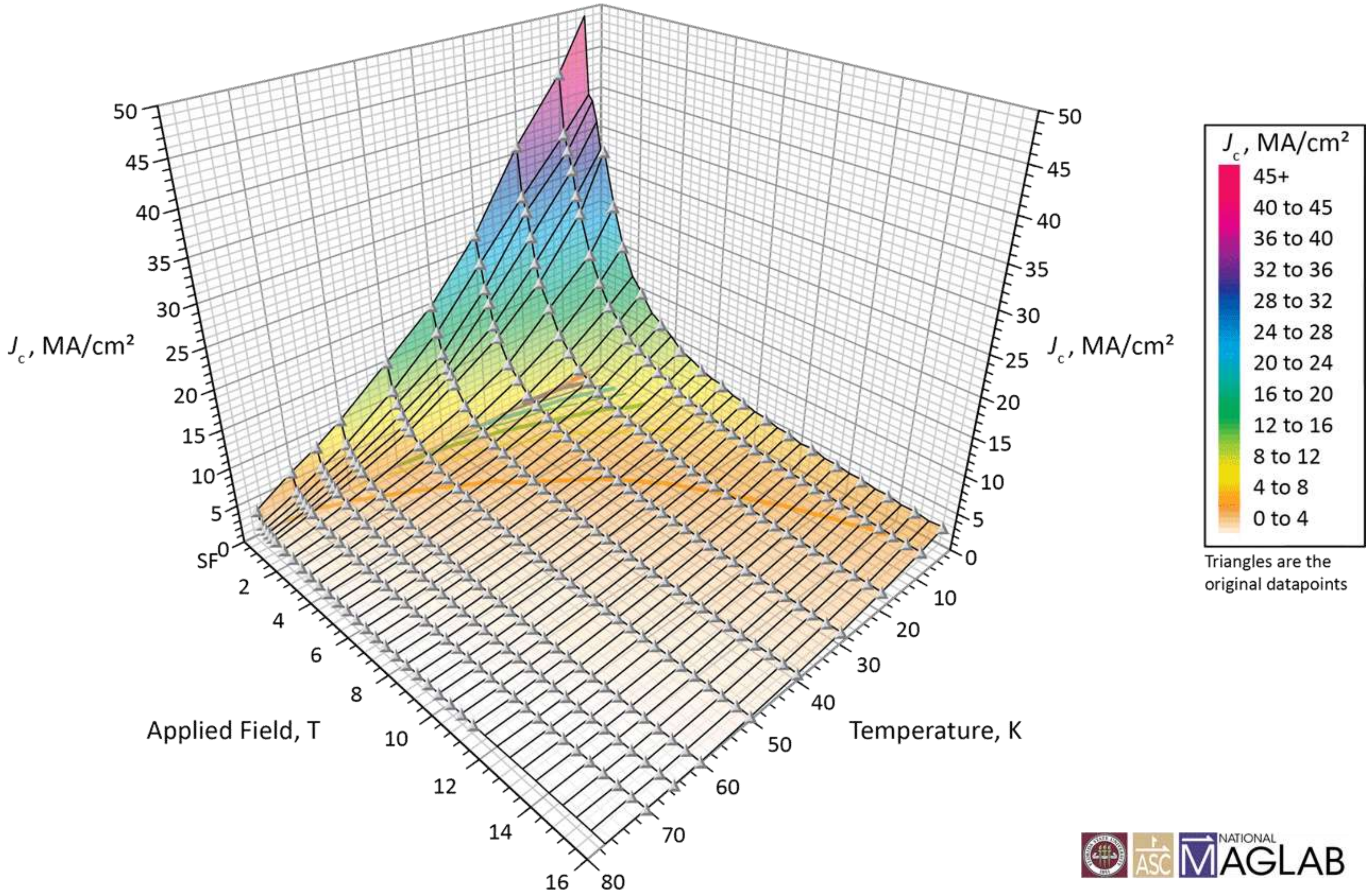

Reference: Superpower YBCO Data Measured at National MagLab by Aixia Xu, March 2011. H ∥ C (⊥ tape surface).

https://nationalmaglab.org/

6.1.2 Materials Requirements

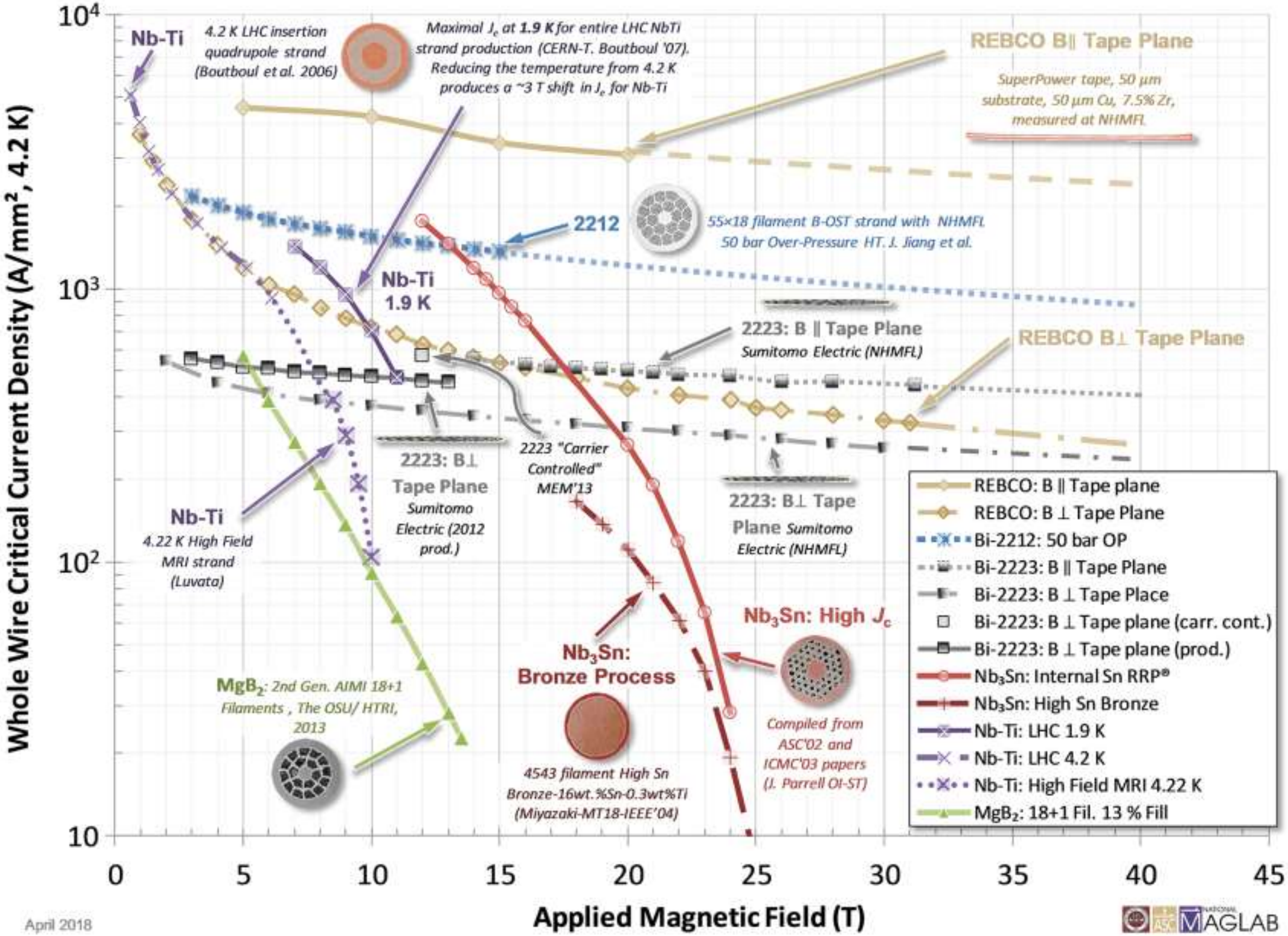

Engineering Critical Current Density vs. Applied Field for Superconductors Available in Long Lengths

April 11, 2018

2018

https://nationalmaglab.org/

References (updated 4/2021)

- YBCO: Tape, ∥ Tape-plane, SuperPower. REBCO: SP26 tape, 50 µm substrate, 7.5%Zr. Measured at NHMFL by Valeria Braccini, Jan Jaroszynski and Aixia Xu: DOI: 10.1088/0953-2048/24/3/035001
- YBCO: Tape, ⊥ Tape-plane. REBCO: SP26 tape, 50 µm substrate, 7.5%Zr. Measured at NHMFL by Valeria Braccini, Jan Jaroszynski and Aixia Xu: DOI: 10.1088/0953-2048/24/3/035001
- Bi-2223: B ∥ Tape plane: Sumitomo Electric Industries. Measured at NHMFL (D. Abraimov) unpublished
- Bi-2223 (Carrier Controlled): B ⊥ Tape-plane "DI" BSCCO "Carrier Controlled" Sumitomo Electric Industries (MEM'13 presented by Kazuhiko Hayashi).
- Bi-2223 (2012 production): B ⊥ Tape-plane "DI" BSCCO (measured at NHMFL by Jianyi Jiang and Dmytro Abraimov Oct. 2013).
- 2212: OST NHMFL 50 bar overpressure HT. Sample pmm170123, 0.78 mm Diam. (after HT) , OST 55x18 composite using nGimat powder. Jiang J, Bradford G, Hossain SI, Brown MD, Cooper J, Miller E, Huang Y, Miao H, Parrell JA, White M, Hunt A, Sengupta S, Revur R, Shen T, Kametani F, Trociewitz UP, Hellstrom EE, Larbalestier DC (2019) High-Performance Bi-2212 Round Wires Made With Recent Powders. IEEE Transactions on Applied Superconductivity, 29(5):1–5. DOI: 10.1109/TASC.2019.2895197
- Nb-47Ti: 0-6 T - Boutboul et al. MT-19: Boutboul, T.; Le Naour, S.; Leroy, D.; Oberli, L.; Previtali, V.; , "Critical Current Density in Superconducting Nb-Ti Strands in the 100 mT to 11 T Applied Field Range," Applied Superconductivity, IEEE Transactions on , vol.16, no.2, pp.1184-1187, June 2006. DOI: 10.1109/TASC.2006.870777
- Nb-47Ti 1.8 K 5-8 T Maximal for whole LHC NbTi strand production (CERN-T. Boutboul '07)
- Nb-47Ti 4.2 K for the LHC insertion quadrupole strand (T. Boutboul, S. Le Naour, D. Leroy, L. Oberli, and V. Previtali, “Critical Current Density in Superconducting Strands in the 100 mT to 11 T Applied Field Range,” IEEE Transactions on Applied Superconductivity, vol. 16, no. 2, pp. 1184–1187, Jun. 2006 DOI: 10.1109/TASC.2006.870777)
- Nb-47Ti 4.22 K for 11.75 T Iseult/INUMAC MRI: Kanithi H, Blasiak D, Lajewski J, Berriaud C, Vedrine P and Gilgrass G 2014 Production Results of 11.75 Tesla Iseult/INUMAC MRI Conductor at Luvata IEEE Transactions on Applied Superconductivity 24 1–4 DOI: 10.1109/TASC.2013.2281417
- Nb_3Sn (RRP®): Non-Cu Jc Internal Sn OI-ST RRP® 1.3 mm, Parrell, J.A.; Youzhu Zhang; Field, M.B.; Cisek, P.; Seung Hong; "High field Nb_3Sn conductor development at Oxford Superconducting Technology," Applied Superconductivity, IEEE Transactions on , vol.13, no.2, pp. 3470- 3473, June 2003.
- DOI: 10.1109/TASC.2003.812360 and Nb_3Sn Conductor Development for Fusion and Particle Accelerator Applications J. A. Parrell, M. B. Field, Y. Zhang, and S. Hong, AIP Conf. Proc. 711, 369 (2004), DOI: 10.1063/1.1774590.
- Nb_3Sn (High Sn Bronze): T. Miyazaki et al. MT18 - fig3, Miyazaki, T.; Kato, H.; Hase, T.; Hamada, M.; Murakami, Y.; Itoh, K.; Kiyoshi, T.; Wada, H.; , "Development of high Sn content bronze processed Nb3Sn superconducting wire for high field magnets," Applied Superconductivity, IEEE Transactions on , vol.14, no.2, pp. 975- 978, June 2004, DOI: 10.1109/TASC.2004.830344
- MgB_2: 18 Filament - The OSU/HTRI C 2 mol% AIMI ("Advanced Internal Mg Infiltration") 33.8 Filament to strand ratio, 39.1% MgB_2 in filament. (DOI: 10.1088/0953-2048/25/11/115023)
- G. Z. Li, M. D. Sumption, J. B. Zwayer, M. A. Susner, M. A. Rindfleisch, C. J. Thong, M. J. Tomsic, and E. W. Collings, “Effects of carbon concentration and filament number on advanced internal Mg infiltration-processed MgB_2 strands,” Superconductor Science and Technology, vol. 26, no. 9, p. 095007, Sep. 2013.

6.1.2 Materials Requirements

critical current density of Fe-based superconductors:

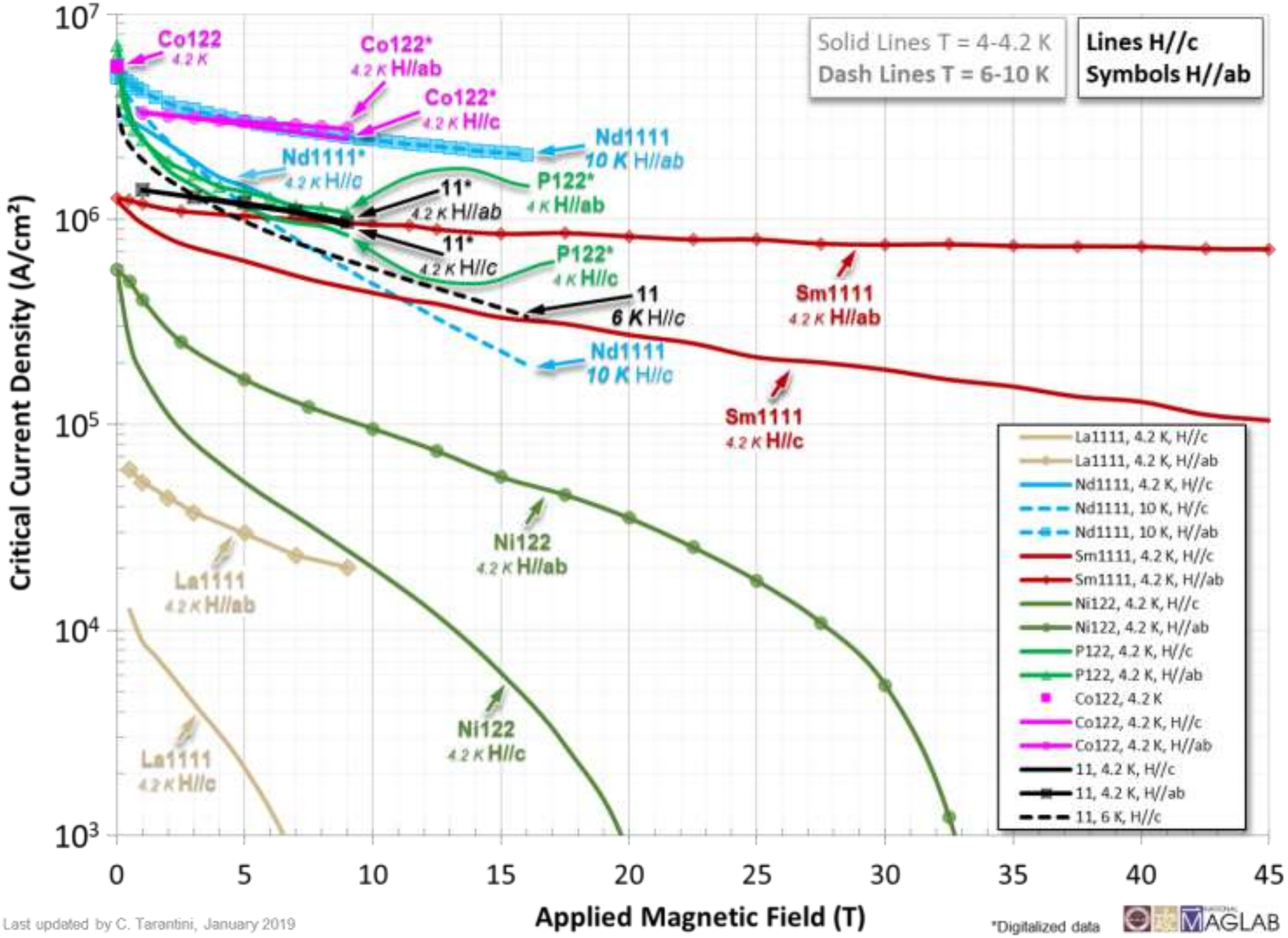

References

- La1111, 4.2 K, H//*c* and H//*ab*: M. Kidszun *et al.* Critical Current Scaling and Anisotropy in Oxypnictide Superconductors, *Phys. Rev. Lett.* **106**, 137001 (2011). https://doi.org/10.1103/PhysRevLett.106.137001
- Nd1111, 4.2 K, H//*c*: M. Chihara *et al.* Direct growth of superconducting NdFeAs(O,F) thin films by MBE, *Phycisa C* **518**, 69-72 (2015). https://doi.org/10.1016/j.physc.2015.03.022
- Nd1111, 10 K, H//*c* and H//*ab*: C. Tarantini *et al.* Effect of α-particle irradiation on a NdFeAs(O,F) thin film, *Supercod. Sci. Technol.* **31**, 034002 (2018). https://doi.org/10.1088/1361-6668/aaa821
- Sm1111, 4.2 K, H//*c* and H//*ab*: K. Iida *et al.* Oxypnictide SmFeAs(O,F) superconductor: a candidate for high–field magnet applications, *Sci. Rep.* **3**, 2139 (2013). https://doi.org/10.1038/srep02139
- Ni122, 4.2 K, H//*c* and H//*ab*: S. Richter *et al.* Superconducting properties of $Ba(Fe_{1-x}Ni_x)_2As_2$ thin films in high magnetic fields, *Appl. Phys. Lett.* **110**, 022601 (2017). http://dx.doi.org/10.1063/1.4973522
- P122, 4.2 K, H//*c* and H//*ab*: H. Sato *et al.* High critical-current density with less anisotropy in $BaFe_2(As,P)_2$ epitaxial thin films: Effect of intentionally grown c-axis vortex-pinning centers, *Appl. Phys. Lett.* **104**, 182603 (2014). http://dx.doi.org/10.1063/1.4875956
- Co122, 4.2 K: C. Tarantini *et al.* Development of very high J_c in $Ba(Fe_{1-x}Co_x)_2As_2$ thin films grown on CaF_2, *Sci. Rep.* **4**, 7305 (2014). https://doi.org/10.1038/srep07305
- Co122, 4.2 K, H//*c* and H//*ab*: P. Yuan *et al.* Vortex pinning properties in Co-doped $BaFe_2As_2$ thin films with a high critical current density over 2 MA cm^{-2} at 9 T, *Supercond. Sci. Technol.* **30**, 025001 (2017). http://dx.doi.org/10.1088/0953-2048/30/2/025001
- 11, 4.2 K, H//*c* and H//*ab*: P. Yuan *et al.* Angular-dependent vortex pinning mechanism and magneto-optical characterizations of $FeSe_{0.5}Te_{0.5}$ thin films grown on CaF_2 substrates, *Supercond. Sci. Technol.* **29**, 035013 (2016). http://dx.doi.org/10.1088/0953-2048/29/3/035013
- 11, 6 K, H//*c*: S. Seo *et al.* Artificially Engineered Nanostrain in Iron Chalcogenide Superconductor Thin Film for Enhancing Supercurrent, arXiv: 1812.02380. https://arxiv.org/abs/1812.02380

https://nationalmaglab.org/

6.1.3 Superconducting Wires and Tapes

fabrication technology for superconducting wires:

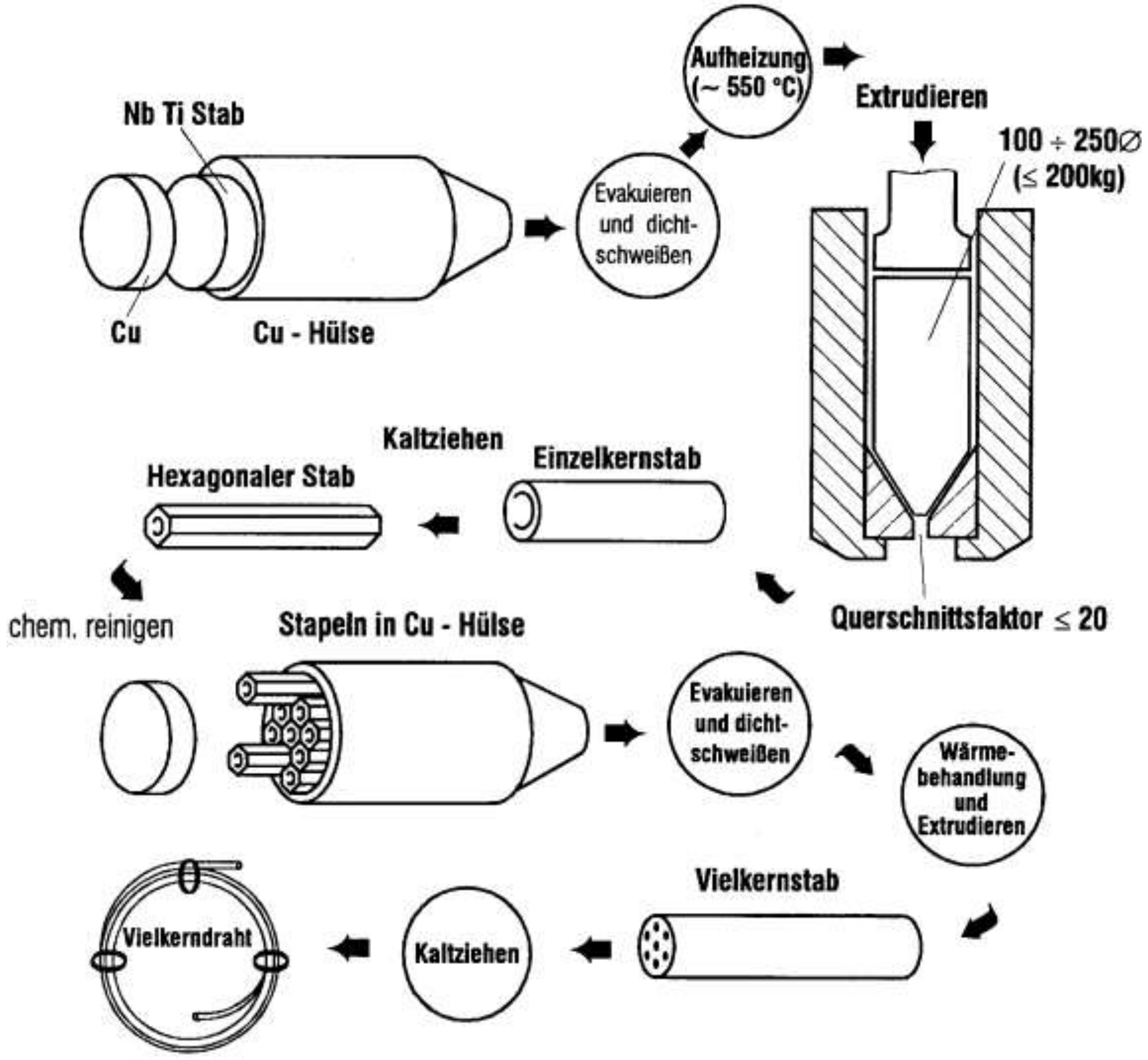

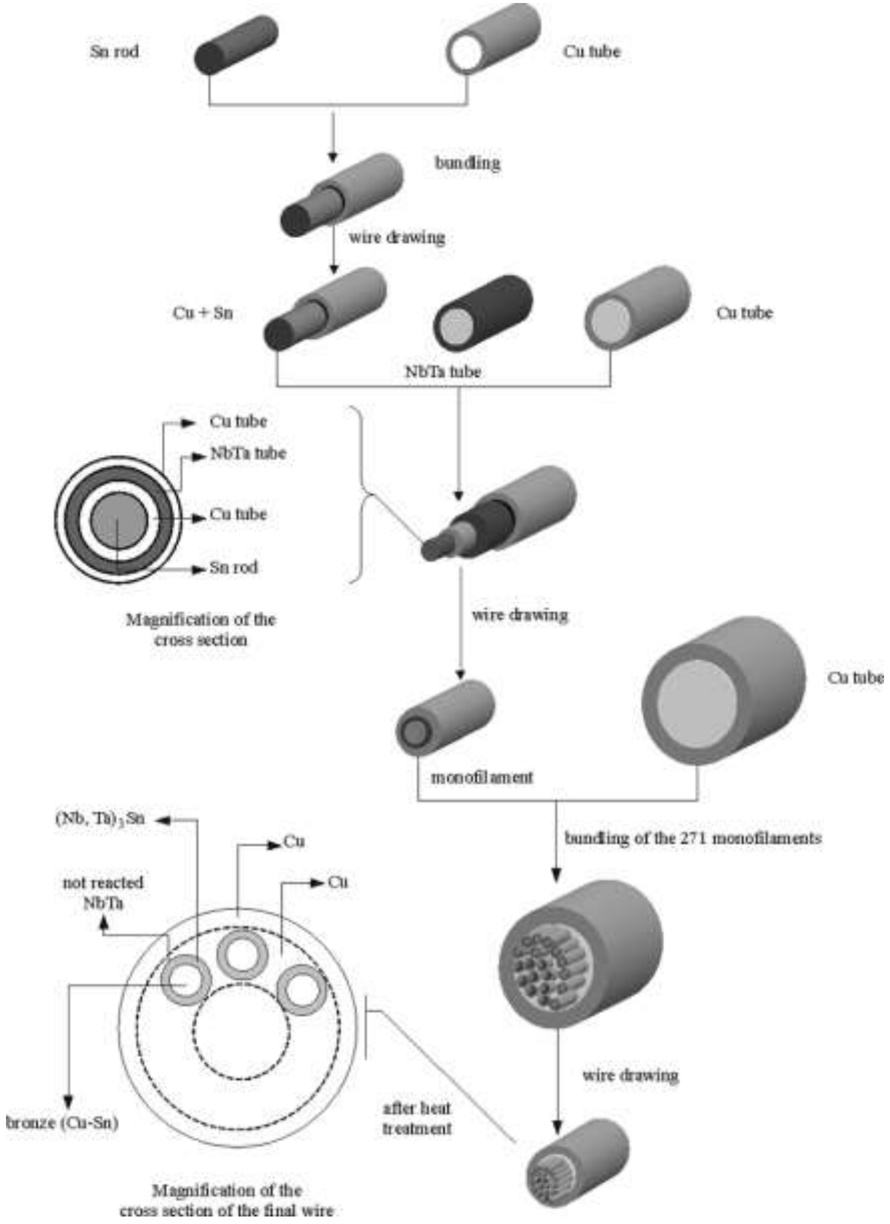

fabrication technology for wires of Fe-based superconductors:

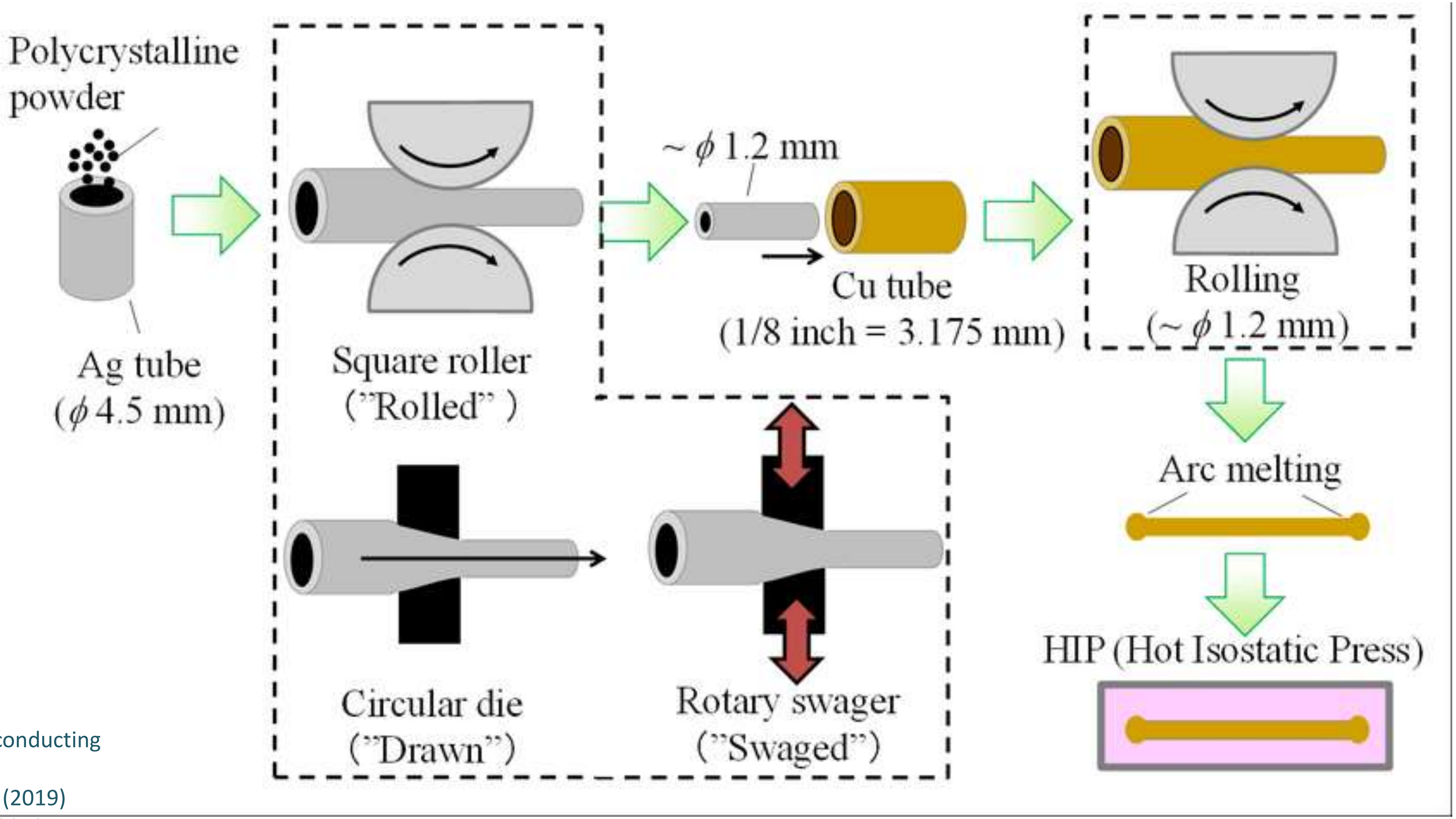

Sunseng Pyon et al.,
Recent Progress of Iron-Based Superconducting Round Wires,
Journal of Physics: Conference Series (2019)
DOI: 10.1088/1742-6596/1293/1/012042

6.1.3 Superconducting Wires and Tapes

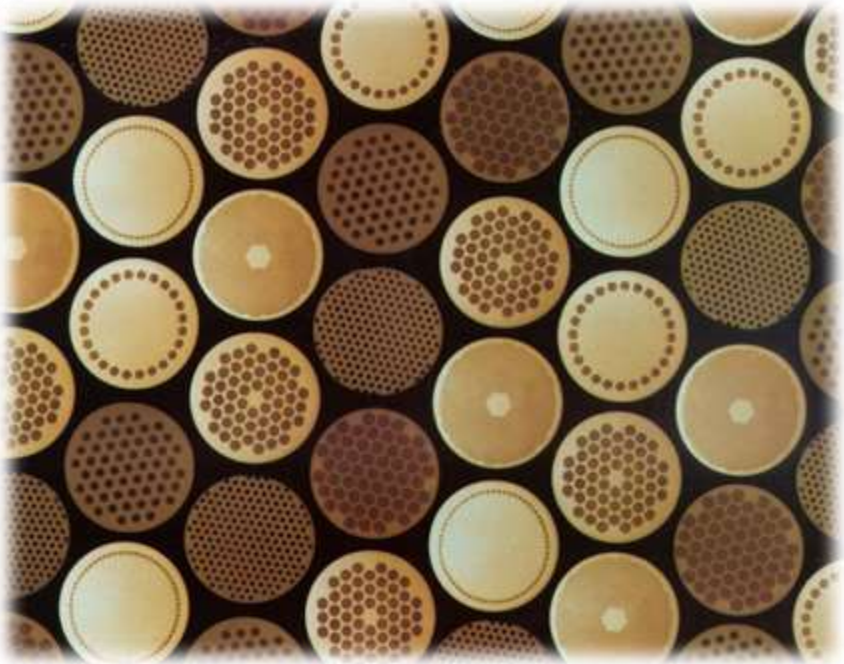

superconducting wires:
NbTi, Nb_3Sn in Cu-matrix

cable from high-T_c superconductor

6.1.3 Superconducting Wires and Tapes

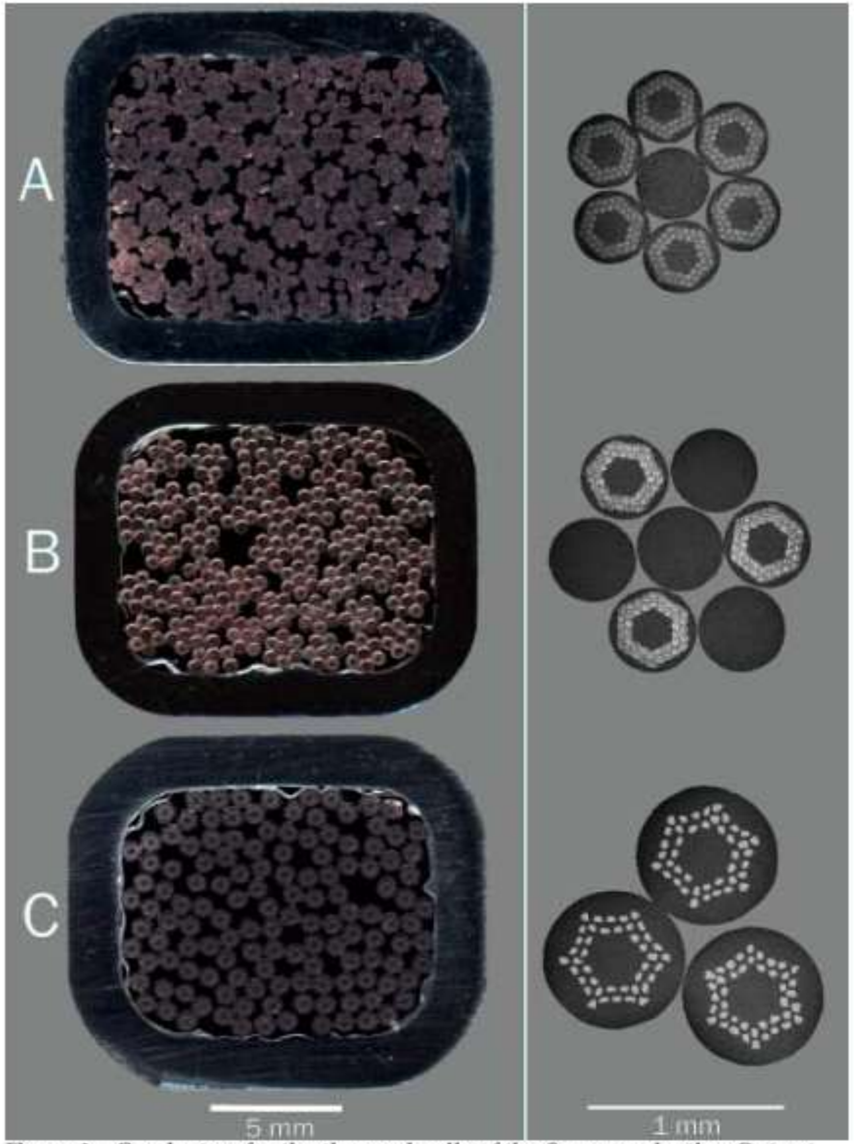

Figure 2 – Conductors for the three subcoils of the Superconducting Outsert Magnet (A, B, and C) were jacketed in special stainless-steel alloys at Gibson Tube. More than 6 km of conductor were used in these coils.

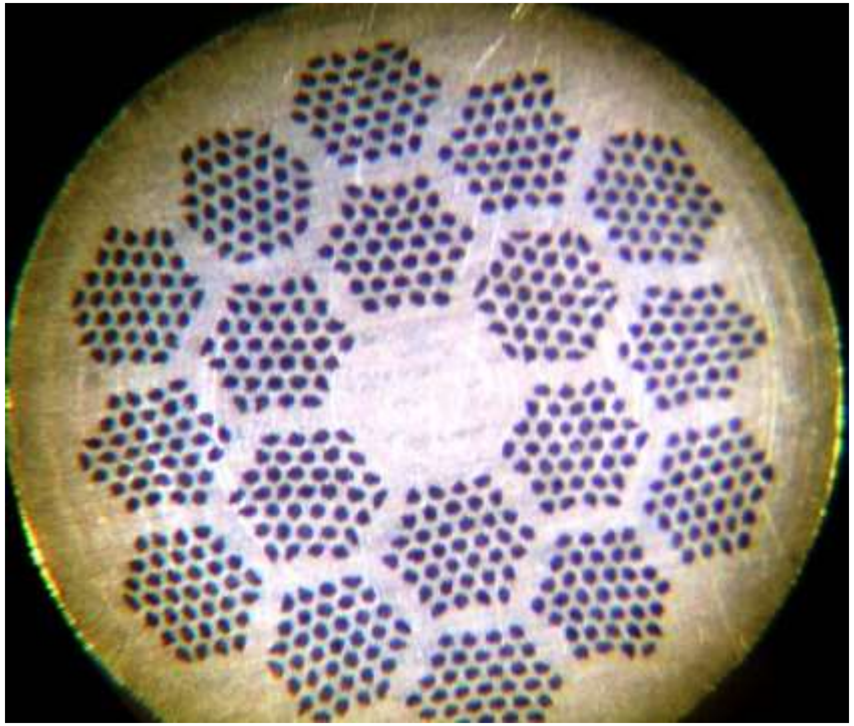

6.1.3 Superconducting Wires and Tapes

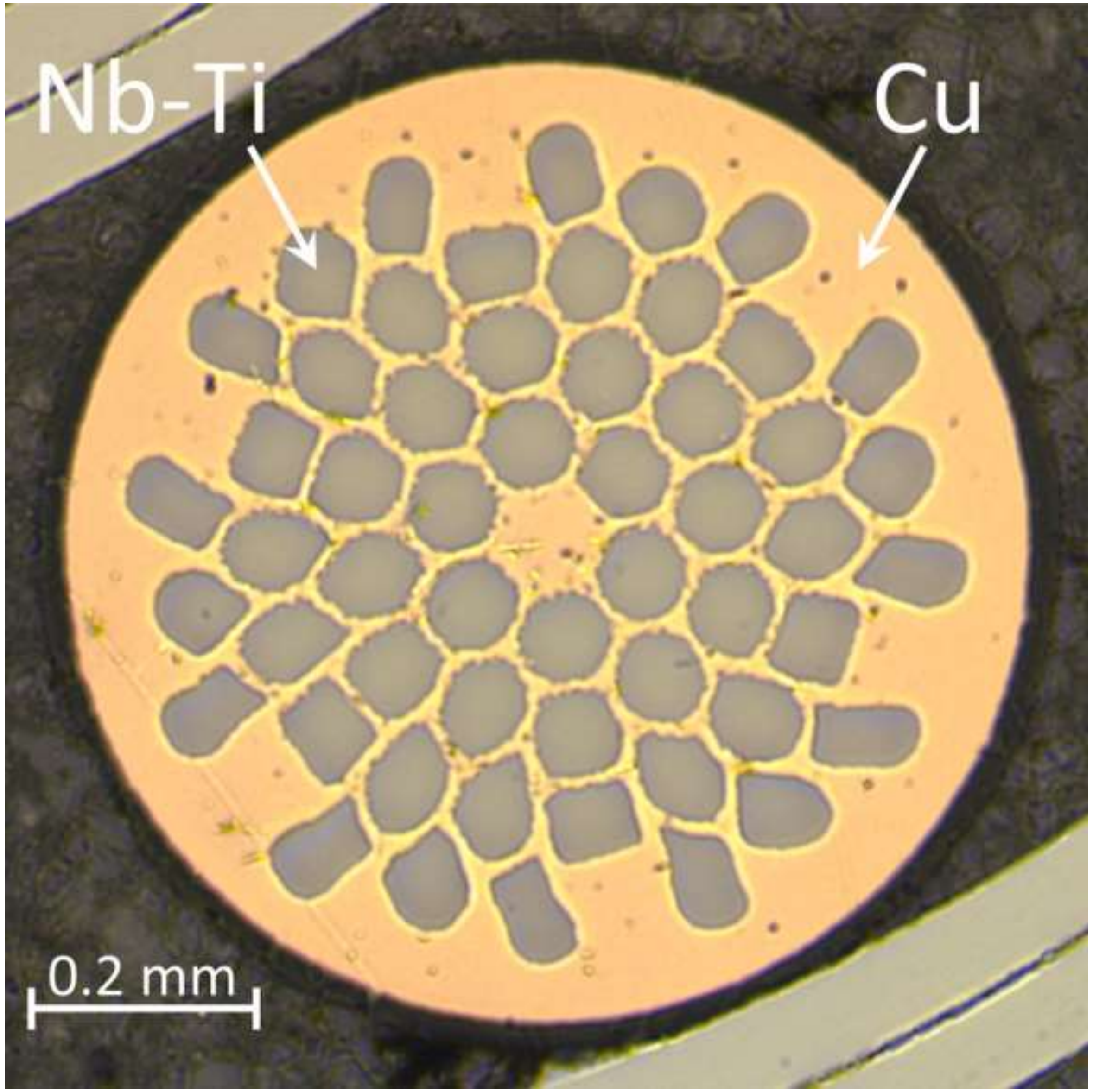

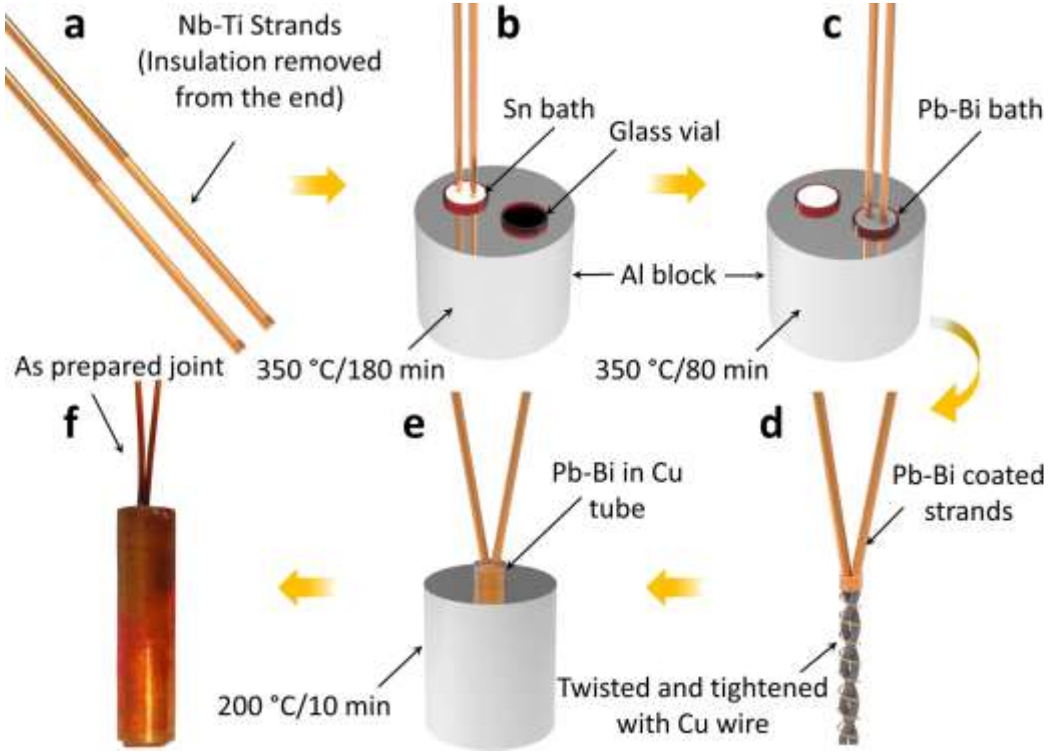

Patel, D., Kim, SH., Qiu, W. *et al.*
Niobium-titanium (Nb-Ti) superconducting joints for persistent-mode operation.
Sci Rep **9,** 14287 (2019).
https://doi.org/10.1038/s41598-019-50549-7

6.1.3 Superconducting Wires and Tapes

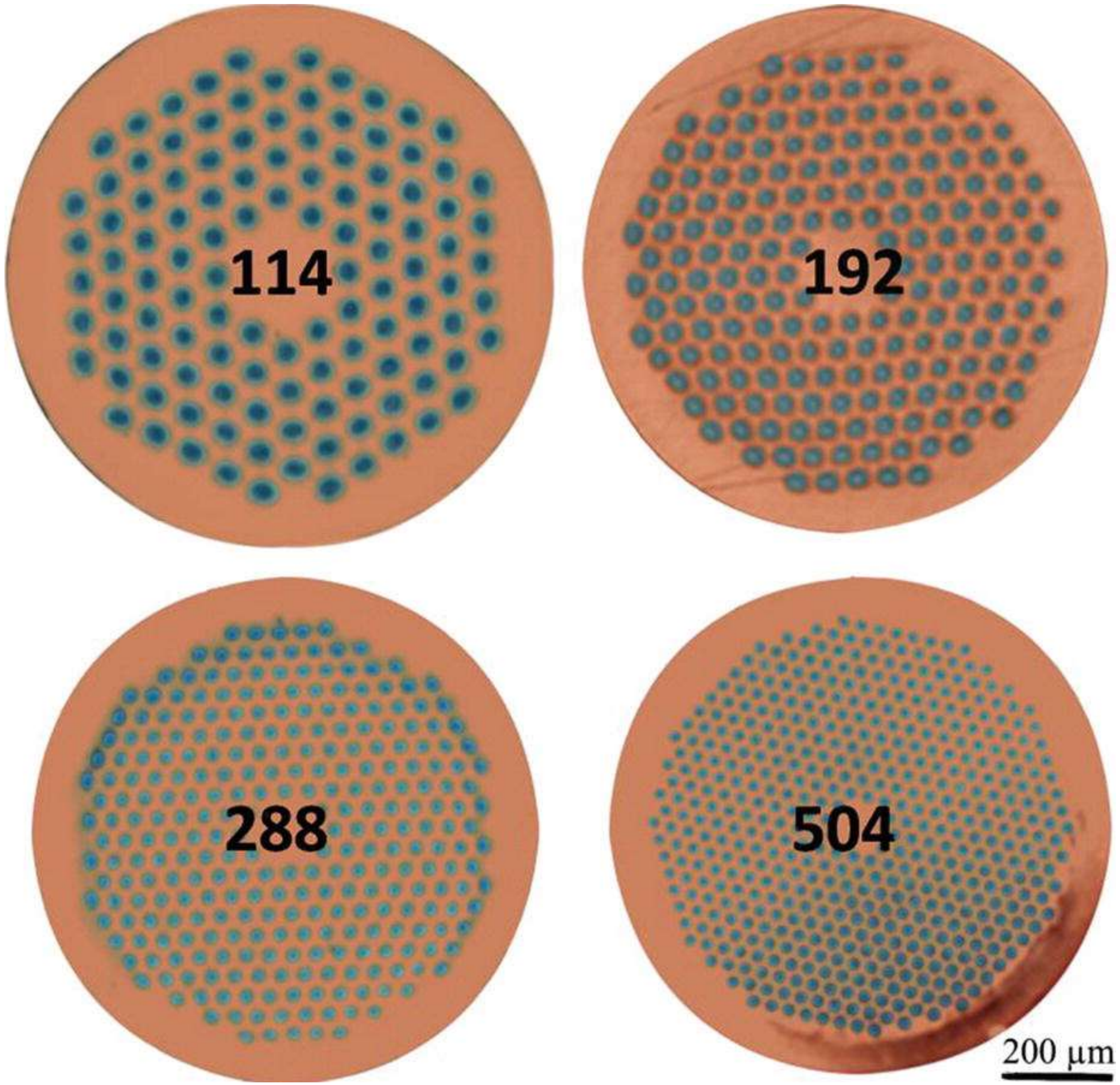

cross-sections of powder-in-tube Nb_3Sn wires of different designs (courtesy of SMI and Bruker-EAS). The numbers represent the total number of superconducting tubes

Barzi E., Zlobin A.V. (2019)
Nb_3Sn Wires and Cables for High-Field Accelerator Magnets.
In: Schoerling D., Zlobin A. (eds) Nb_3Sn Accelerator Magnets. Particle Acceleration and Detection. Springer, Cham.
https://doi.org/10.1007/978-3-030-16118-7_2

6.1.3 Superconducting Wires and Tapes

https://sumitomoelectric.com/

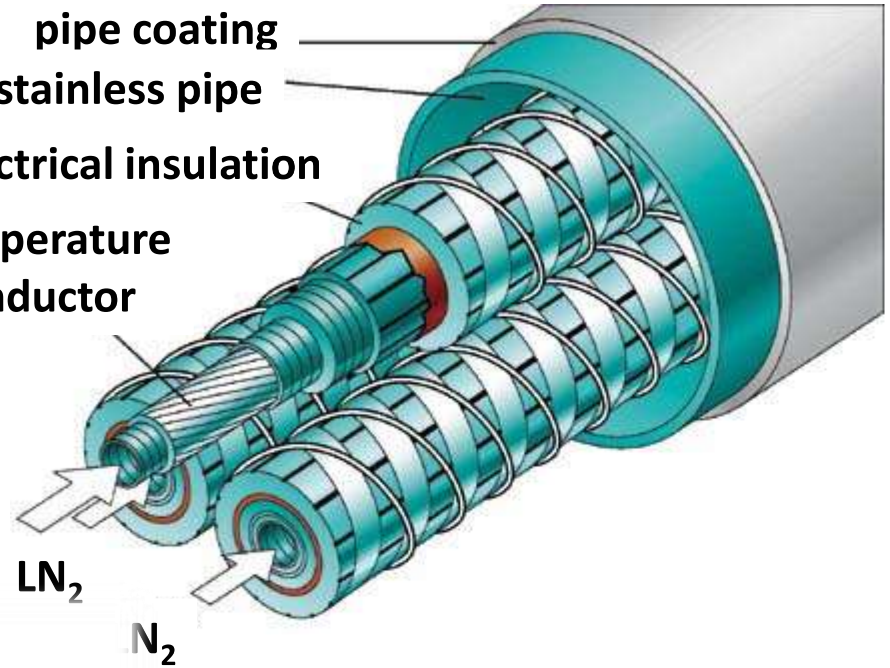

https://www.nexans.com/

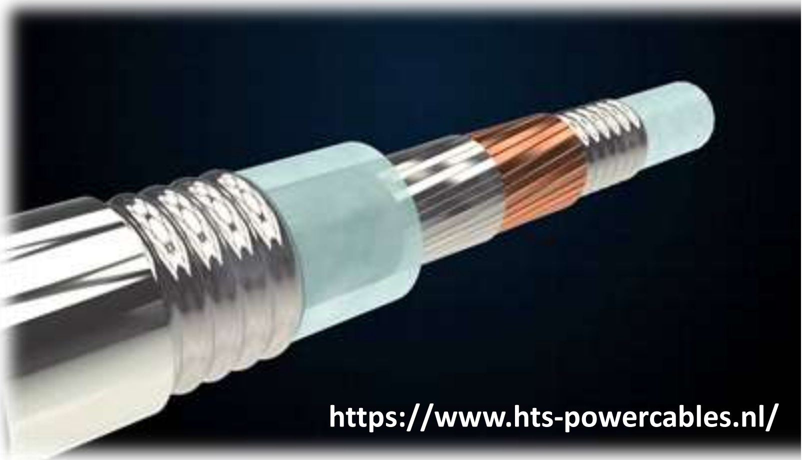

https://www.hts-powercables.nl/

6.1.3 Superconducting Wires and Tapes

high-T_c superconducting wires:

can be made

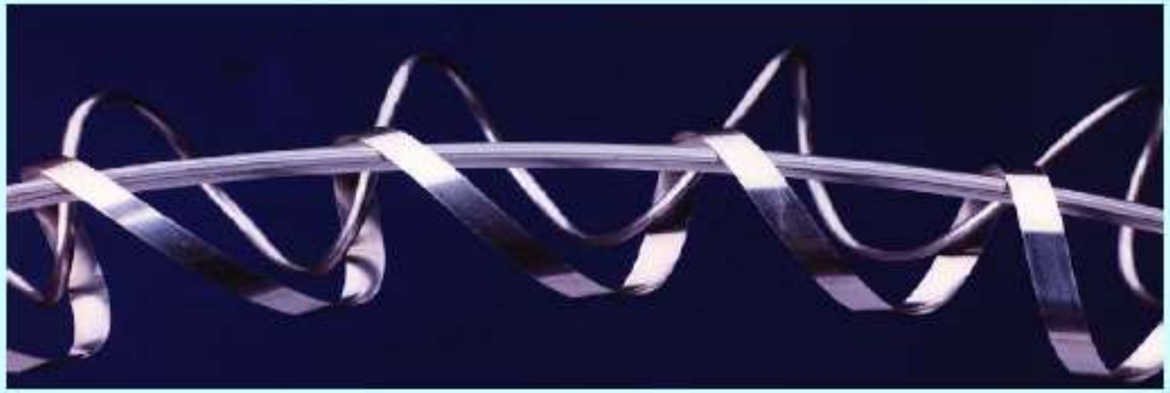

But it's 70% silver!

- Ag is too expensive and too soft
- HTS have higher critical fields

6.1.3 Superconducting Wires and Tapes

preparation of multi-filamentary BiSrCaCu-oxid (2223) tapes in Ag/AgMg-sheath by the powder in tube method
Investigation of the structural and superconducting properties

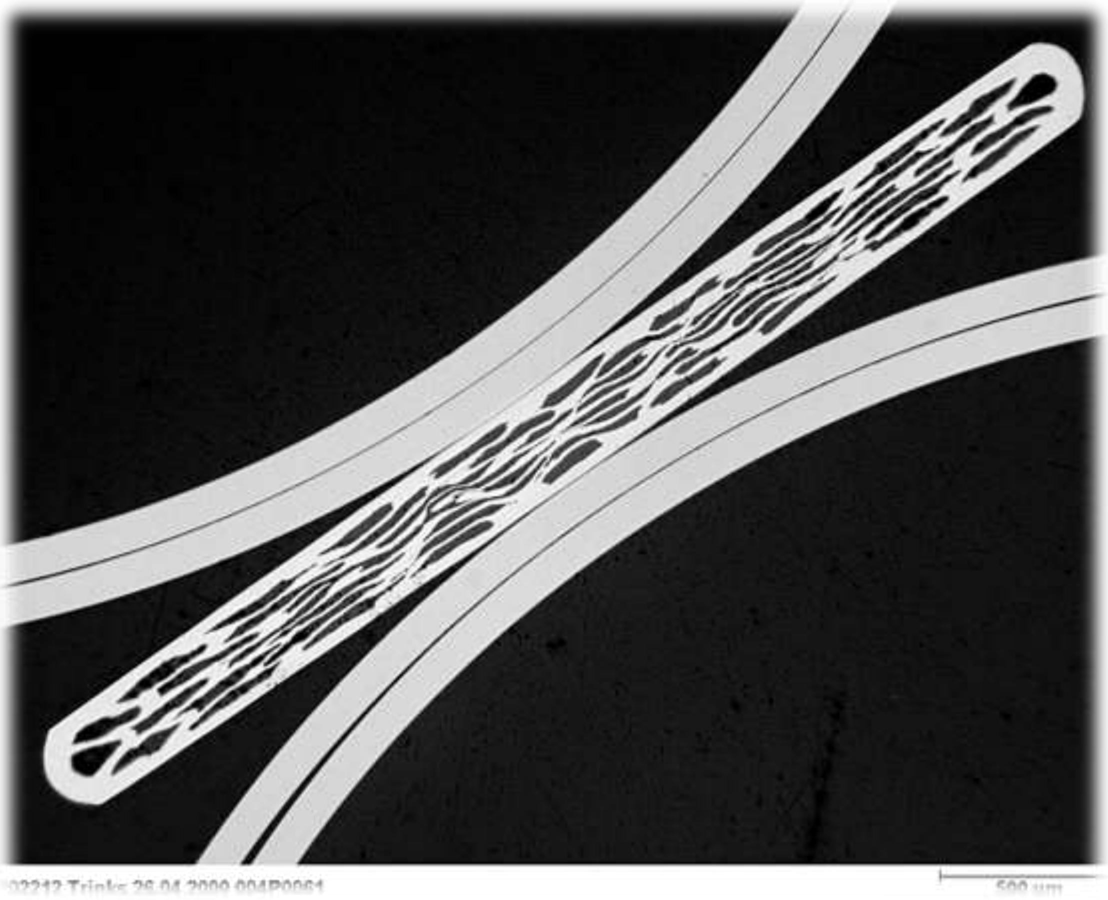

cross-section of 61 filamentary tape

600 m tape on a coil for J_c-measurement

Leibniz-Institut
für Festkörper- und
Werkstoffforschung
Dresden

6.1.3 Superconducting Wires and Tapes

R. Gross and A. Marx , © Walther-Meißner-Institut (2004 - 2022)

HTS cable

6.1.3 Superconducting Wires and Tapes

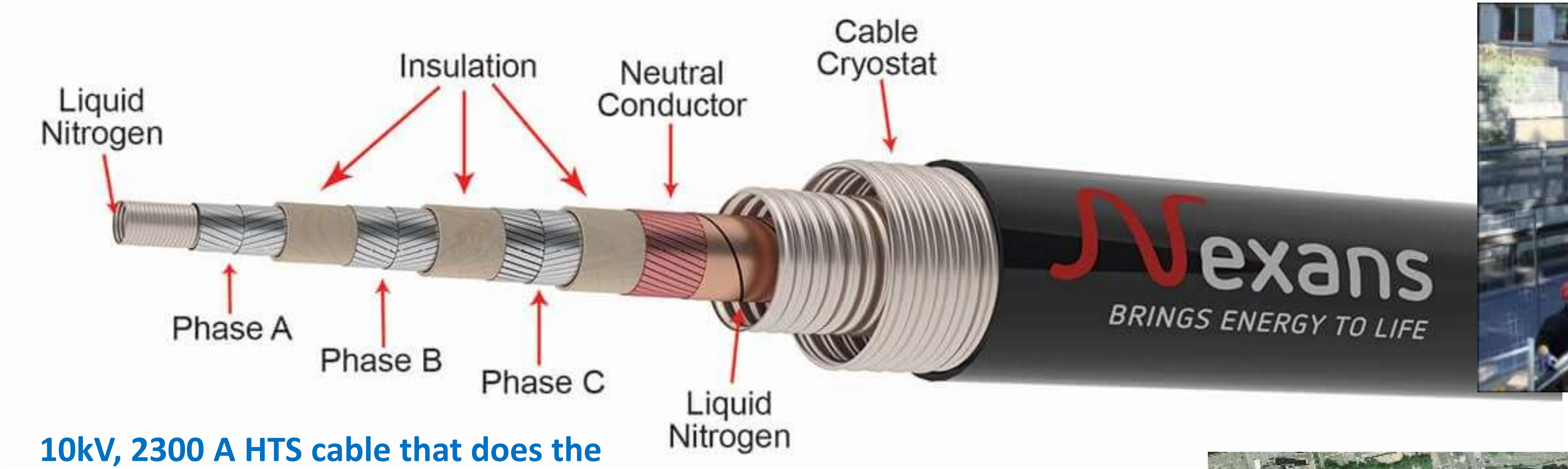

10kV, 2300 A HTS cable that does the same job as a 100 kV conventional cable. This cable has now been in continuous use for six years (2021).

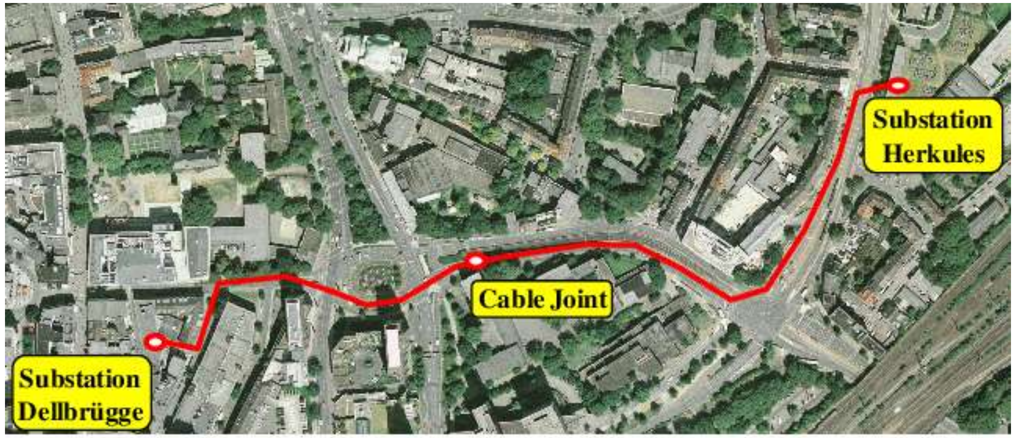

19. January 2012

The "**AmpaCity**" project has been kicked off:
The RWE Group and its partners are just about to replace a 1-kilometre-long high-voltage cable connecting two transformer stations in the Ruhr city of Essen with a state-of-the-art superconductor solution. This will mark the ***longest superconductor cable installation in the world***. As part of this project, the Karlsruhe Institute of Technology will analyse suitable superconducting and insulating materials.

The three-phase, concentric 10 kV cable will be produced by Nexans and is designed for a transmission capacity of 40 megawatts.

6.1.3 Superconducting Wires and Tapes

October 23, 2020:
Stadtwerke München and five cooperation partners have the green light to start development and testing of the components for a 12-kilometer superconductor cable in Munich as part of the **SuperLink project**.

In order to ensure that all components are optimally matched from the outset, the three companies **Linde** for the cooling technology, **NKT** for the cable and **THEVA** for the superconductor are involved.

6.1.3 Superconducting Wires and Tapes

WMI > READ MORE NEWS > CONTACTLESS HIGH PERFORMACE POWER TRASNMISSION

Contactless High Performance Power Transmission

12 March 2021

Superconducting coils boost performance of contactless power transmission

A team led by Technical University of Munich (TUM) physicists Christoph Utschick and Prof. Rudolf Gross has succeeded in making a coil with superconducting wires capable of transmitting power in the range of more than five kilowatts contactless and with only small losses. The wide field of conceivable applications include autonomous industrial robots, medical equipment, vehicles and even aircraft.

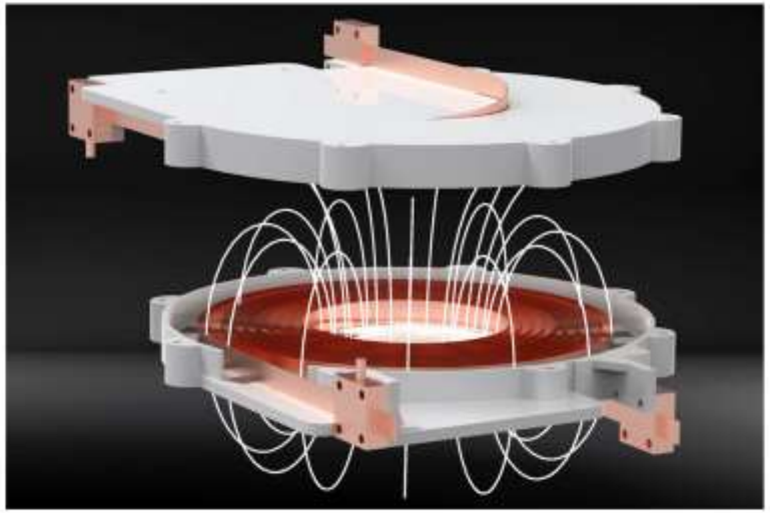

A team led by the physicists Christoph Utschick and Prof. Dr. Rudolf Gross from Walther-Meißner-Institute (WMI) has developed a coil made of superconducting wires that can contactlessly transmit power of more than five kilowatts without major losses (Image: C. Utschick / Würth Elektronik eiSos)

Contactless power transmission has already established itself as a key technology when it comes to charging small devices such as mobile telephones and electric toothbrushes. Users would also like to see contactless charging made available for larger electric machines such as industrial robots, medical equipment and electric vehicles.

Such devices could be placed on a charging station whenever they are not in use. This would make it possible to effectively utilize even short idle times to recharge their batteries. However, the currently available transmission systems for high performance recharging in the kilowatt range and above are large and heavy, since they are based on copper coils.

Working in a research partnership with the companies Würth Elektronik eiSos and superconductor coating specialist Theva Dünnschichttechnik, a team of physicists led by Christoph Utschick and **Rudolf Gross** have succeeded in creating a coil with superconducting wires capable of contactless power transmission in the order of more than five kilowatts (kW) and without significant loss.

https://www.wmi.badw.de/news-1/contactless-high-performace-power-trasnmission#c126

6.1.3 Superconducting Wires and Tapes

"Garching-technology„ for HTS tapes:

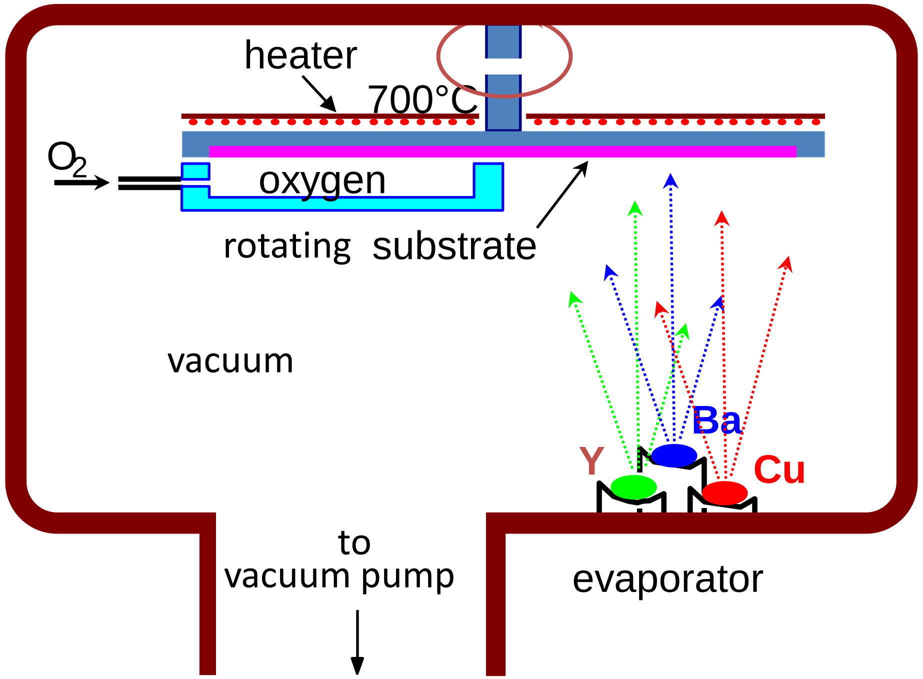

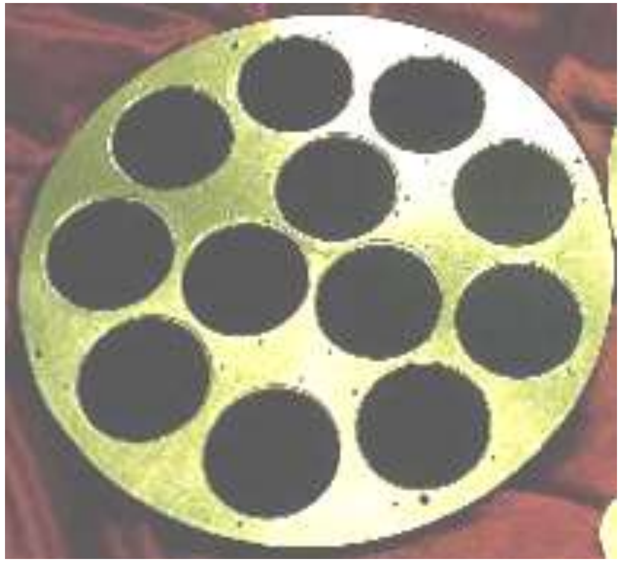

230 mm

http://www.theva.com/

- **low cost process for large area deposition of HTS films**
- **high quality and reproducibility**

THEVA coated conductors

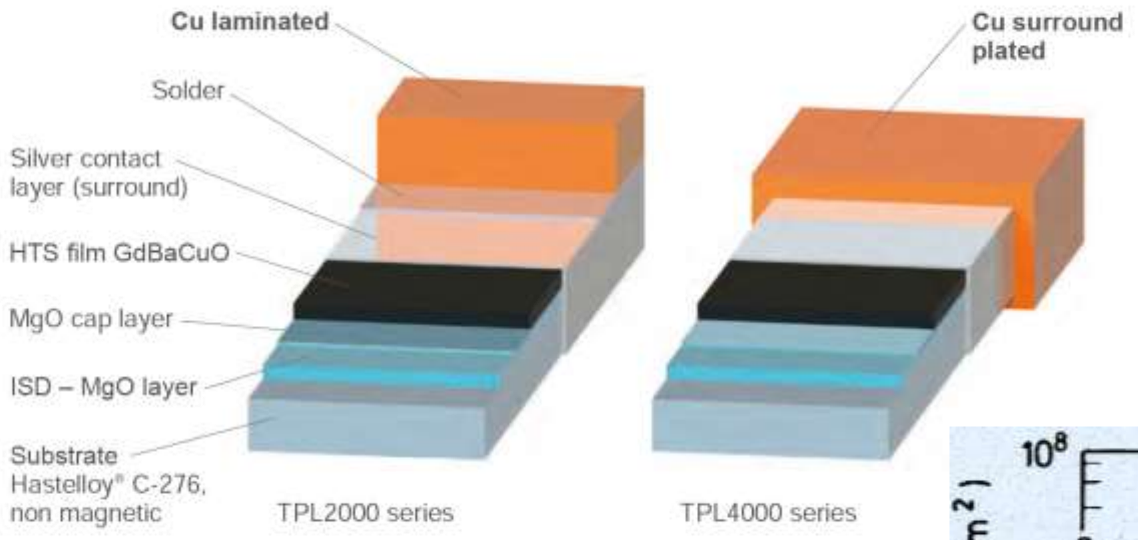

coated conductor:

superconducting film on flexible steel tape

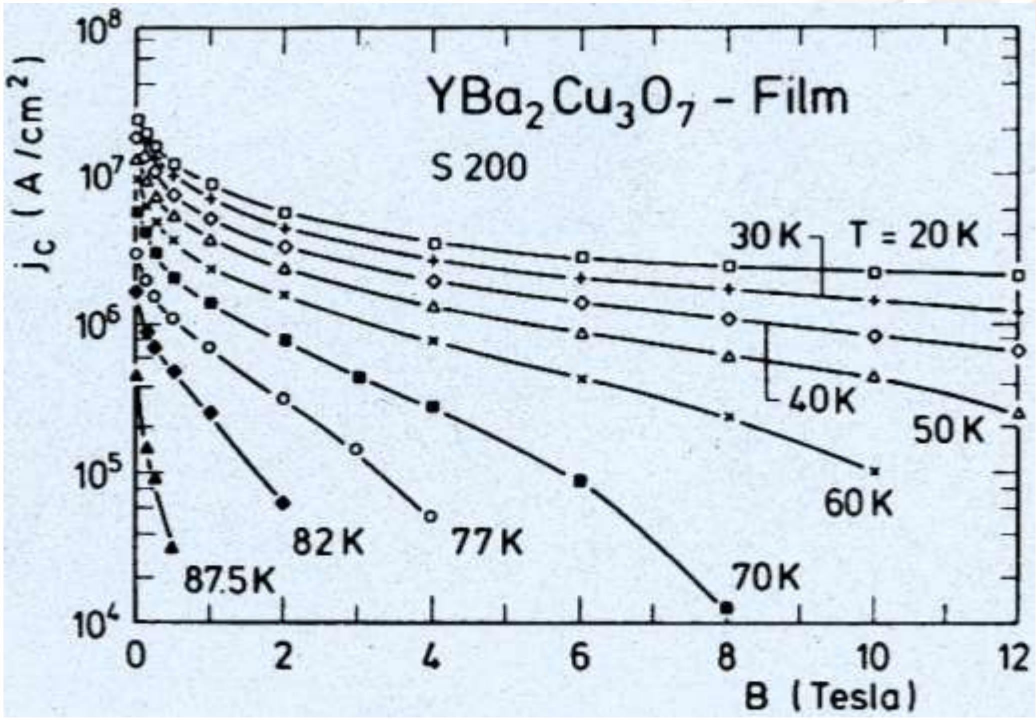

R. Gross and A. Marx , © Walther-Meißner-Institut (2004 - 2022)

6.1.4 Superconducting Bulk Material

bulk superconductors as “permanent magnets”

6.1.4 Superconducting Bulk Material

6.1.4 Superconducting Bulk Material

6.1.4 Superconducting Bulk Material

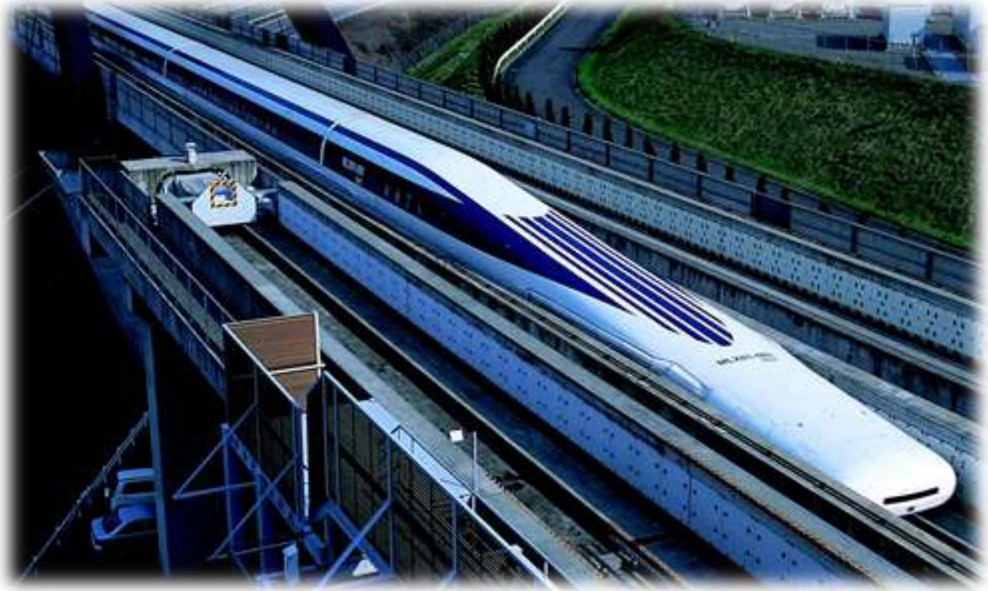

MLX01-901

Jap. Yamanashi MAGLEV-System

(42.8 km long test track between Sakaigawa and Akiyama)

maximum velocity:
581 km/h (02. 12. 2003)

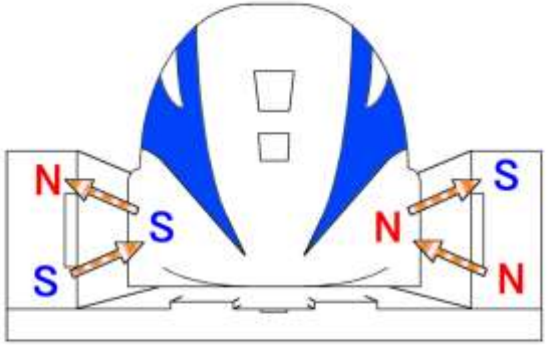

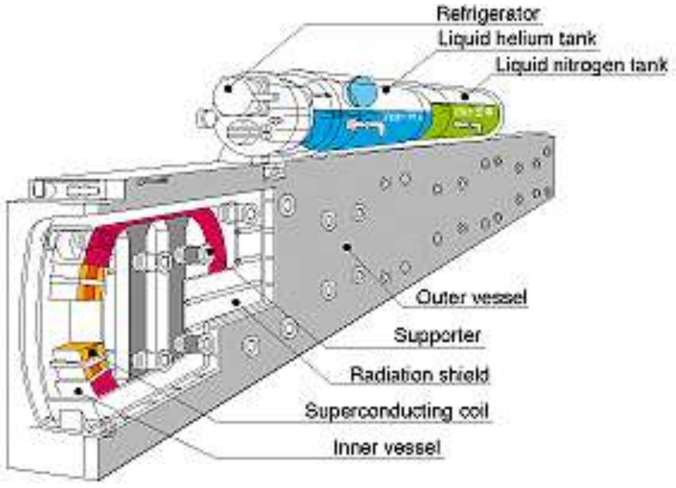

Magnetization Curve for a Superconducting Slab

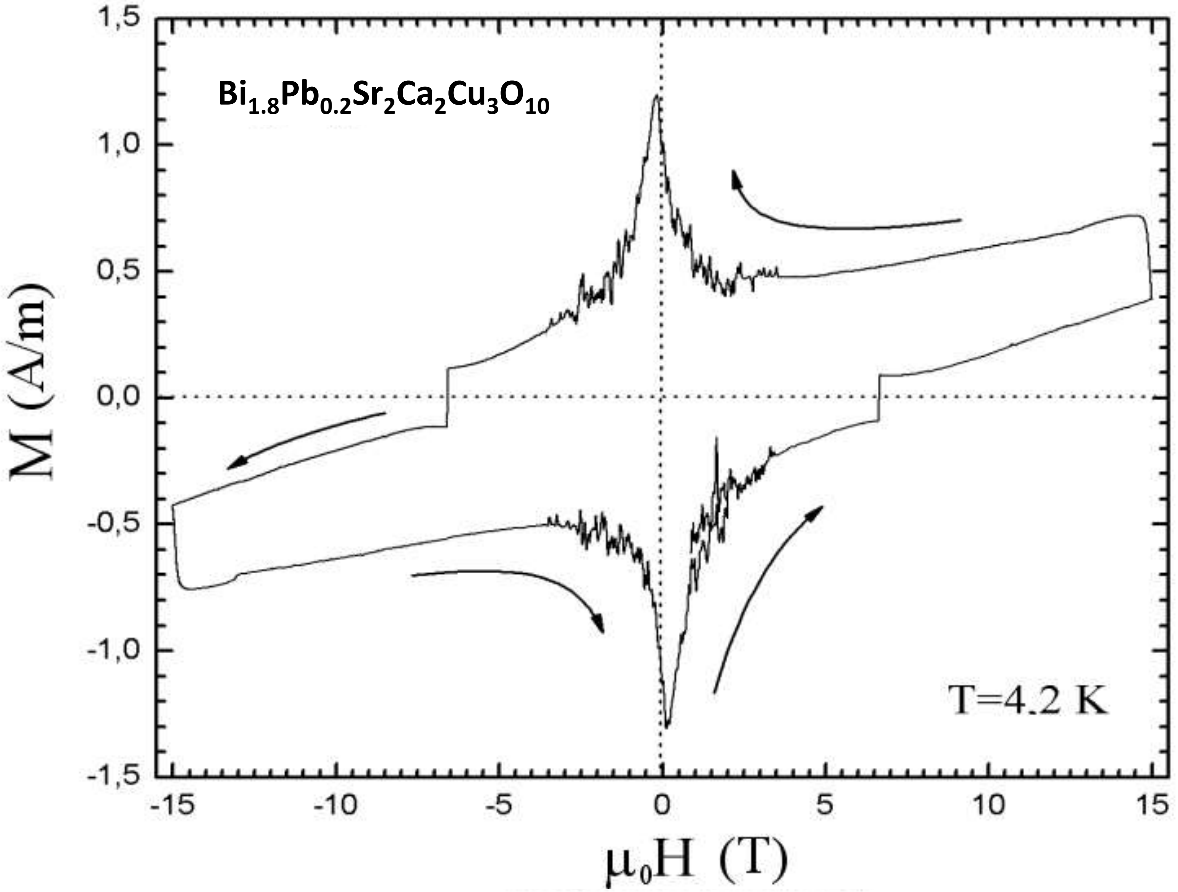

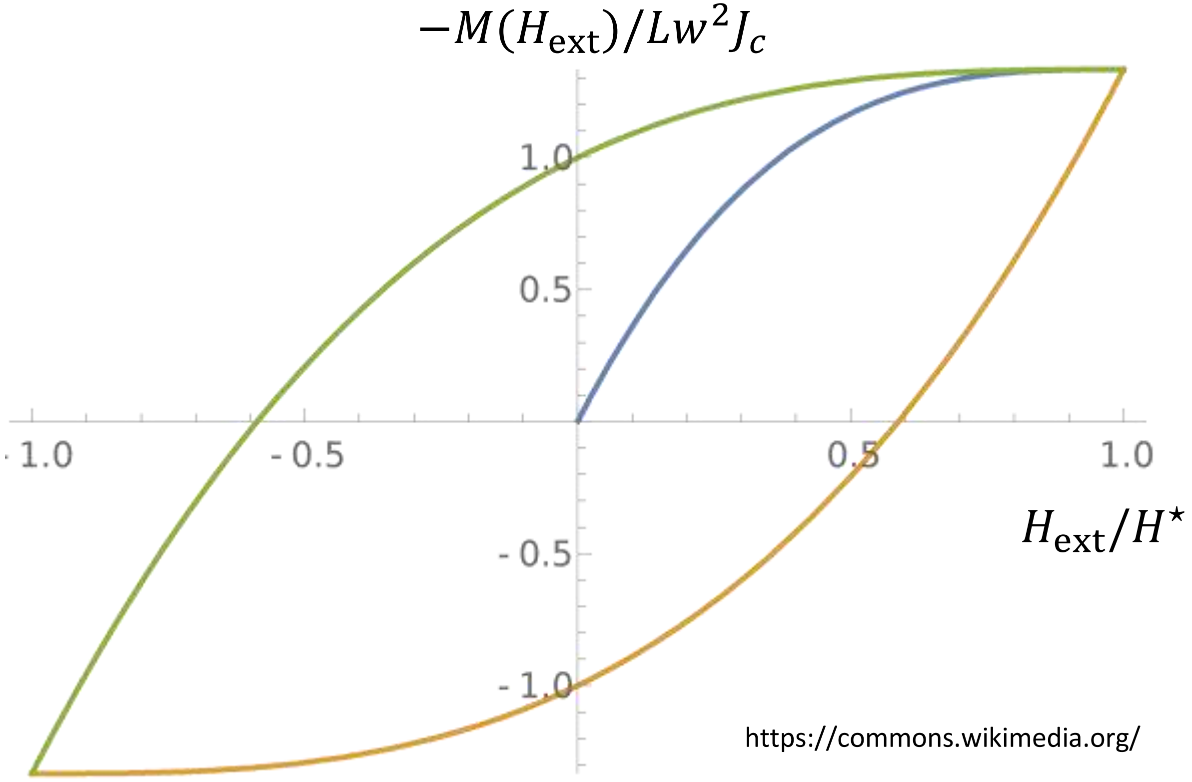

https://commons.wikimedia.org/

6 Flux Pinning and Critical Currents

6.2 Critical Current of Superconductors

critical current density of type-II superconductors is limited by different physical effects

- increase of supercurrent density results in increase of velocity of superconducting electrons

  critical current density: **kinetic energy = binding energy of Cooper pairs**

  ➡ ***depairing critical current density***

- increase of supercurrent results in Lorentz force on flux lines in mixed state of type-II superconductors

  critical current density: **Lorentz force = pinning force**

  ➡ ***depinning critical current density***

revision: Ginzburg-Landau theory (cf. 3.3)

- minimization of free enthalpy of superconductor:
  → integration of enthalpy density over whole volume of superconductor
  → minimization by variation of $\Psi(\mathbf{r})$ and $\mathbf{A}(\mathbf{r})$

Ginzburg-Landau equations:

$$\frac{1}{2m_s}\left(\frac{\hbar}{\imath}\boldsymbol{\nabla} - q_s\,\mathbf{A}(\mathbf{r})\right)^2 \Psi(\mathbf{r}) + \alpha\Psi(\mathbf{r}) + \frac{1}{2}\beta|\Psi(\mathbf{r})|^2\Psi(\mathbf{r}) = 0$$

1st Ginzburg-Landau equation

$$\mathbf{J}_s = \frac{q_s\hbar}{2m_s\imath}(\Psi^\star\boldsymbol{\nabla}\Psi - \Psi\boldsymbol{\nabla}\Psi^\star) - \frac{q_s^2}{m_s}|\Psi|^2\mathbf{A}$$

2nd Ginzburg-Landau equation

$$\lambda_{\mathrm{GL}} = \sqrt{\frac{m_s}{\mu_0 n_s q_s^2}}$$

GL penetration depth

$$\xi_{\mathrm{GL}} = \sqrt{\frac{\hbar^2}{2m_s|\alpha|}}$$

GL coherence length

6.2.1 Depairing Critical Current Density

derivation of the depairing critical current density from the GL equations

- simplifying assupmtions:
  - consider a thin wire with diameter $d \ll \xi_{\mathrm{GL}}$ → no amplitude variation of order parameter Ψ across wire
  - superconducting material is assumed homogeneous → same current density along the wire → no amplitude variation of order parameter Ψ along the wire

$$\Rightarrow \Psi(\mathbf{r}) = \Psi_0 \, \mathrm{e}^{\imath\theta(\mathbf{r})}$$

- we use 1. and 2. GL equation:

$$\mathbf{J}_s = \frac{q_s \hbar}{2 m_s \imath}(\Psi^\star \nabla \Psi - \Psi \nabla \Psi^\star) - \frac{q_s^2}{m_s}|\Psi|^2 \mathbf{A} \underset{\Psi(\mathbf{r}) = \Psi_0 \, \mathrm{e}^{\imath\theta(\mathbf{r})}}{\underbrace{\Rightarrow}} \mathbf{J}_s = q_s n_s \underbrace{\left\{\frac{\hbar}{m_s}\nabla\theta(\mathbf{r}) - \frac{q_s}{m_s}\mathbf{A}(\mathbf{r})\right\}}_{\mathbf{v}_s} = q_s n_s \mathbf{v}_s \qquad \text{with } n_s = |\Psi|^2$$

$$\frac{1}{2m_s}\left(\frac{\hbar}{\imath}\nabla - q_s \mathbf{A}(\mathbf{r})\right)^2 \Psi(\mathbf{r}) + \alpha \Psi(\mathbf{r}) + \frac{1}{2}\beta|\Psi(\mathbf{r})|^2\Psi(\mathbf{r}) = 0 \underset{\tilde{\Psi}(\mathbf{r}) = |\Psi/\Psi_0|}{\underbrace{\Rightarrow}} 0 = -\xi_{\mathrm{GL}}^2\left(\frac{\hbar}{\imath}\nabla - q_s \mathbf{A}(\mathbf{r})\right)^2 \tilde{\Psi} + \tilde{\Psi} - \left|\tilde{\Psi}\right|^2 \tilde{\Psi}$$

$$\text{with } |\Psi|^2 = -\frac{\alpha}{\beta}$$

$$\Rightarrow \quad 0 = -\frac{\xi_{\mathrm{GL}}^2 m_s^2}{\hbar^2}\underbrace{\left\{\frac{\hbar}{m_s}\nabla\theta(\mathbf{r}) - \frac{q_s}{m_s}\mathbf{A}(\mathbf{r})\right\}}_{\mathbf{v}_s}^2 \tilde{\Psi} + \tilde{\Psi} - \left|\tilde{\Psi}\right|^2 \tilde{\Psi}$$

6.2.1 Depairing Critical Current Density

- resolving for $\left|\widetilde{\Psi}\right|^2$ yields

$$\left|\widetilde{\Psi}\right|^2 = 1 - \frac{\xi_{\mathrm{GL}}^2 m_s^2}{\hbar^2} v_s^2 \underbrace{=}_{\xi_{\mathrm{GL}}^2 = \frac{\hbar^2}{2 m_s |\alpha|}} 1 - \frac{\frac{1}{2} m_s v_s^2}{|\alpha|}$$

condensation energy per Cooper pair

➔ reduction of $\left|\widetilde{\Psi}\right|^2$ is just proportional to ratio of ***kinetic*** and ***condensation energy***

→ **order parameter decreases due to additional kinetic energy of pairs**

- expression for current density:

$$\mathbf{J}_s = q_s n_s \mathbf{v}_s = q_s |\Psi|^2 \mathbf{v}_s = q_s \left|\widetilde{\Psi}\right|^2 |\Psi_0|^2 \mathbf{v}_s = q_s |\Psi_0|^2 \left(1 - \frac{\xi_{\mathrm{GL}}^2 m_s^2}{\hbar^2} v_s^2\right) \mathbf{v}_s$$

- determine maximum of J_s by setting $\partial J_s / \partial v_s = 0$:

$$\boxed{J_c^{\mathrm{GL}} = \frac{2}{3\sqrt{3}} \frac{\hbar q_s^2}{m_s \xi_{\mathrm{GL}}} |\Psi_0|^2 = \frac{\Phi_0}{3\pi\sqrt{3}\, \mu_0 \lambda_{\mathrm{L}}^2 \xi_{\mathrm{GL}}}}$$

GL depairing critical current density

$\Phi_0 = h/2e$

$\lambda_{\mathrm{L}}^2 = m_s / \mu_0 |\Psi_0|^2 q_s^2$

6.2.1 Depairing Critical Current Density

$$J_c^{\mathrm{GL}} = \frac{2}{3\sqrt{3}} \frac{\hbar q_s^2}{m_s \xi_{\mathrm{GL}}} |\Psi_0|^2 = \frac{\Phi_0}{3\pi\sqrt{3}\,\mu_0 \lambda_{\mathrm{L}}^2 \xi_{\mathrm{GL}}}$$

- T-dependence of J_c^{GL} is determined by T-dependence of λ_{L} and ξ_{GL}:

close to T_c:

$$\lambda_{\mathrm{GL}}(T) = \frac{\lambda_{\mathrm{GL}}(0)}{\sqrt{1 - \frac{T}{T_c}}}$$

$$\xi_{\mathrm{GL}}(T) = \frac{\xi_{\mathrm{GL}}(0)}{\sqrt{1 - \frac{T}{T_c}}}$$

$\Rightarrow$ $$J_c^{\mathrm{GL}} \propto \frac{1}{\lambda_{\mathrm{L}}^2 \xi_{\mathrm{GL}}} \propto \left(1 - \frac{T}{T_c}\right)^{3/2}$$

- we can use $B_{\mathrm{cth}}(T) = \dfrac{\Phi_0}{2\pi\sqrt{2}\ \xi_{\mathrm{GL}}(T)\,\lambda_{\mathrm{GL}}(T)}$

$\Rightarrow$ $$J_c^{\mathrm{GL}} = \frac{2\sqrt{2}}{3\sqrt{3}} \frac{B_{\mathrm{cth}}}{\mu_0 \lambda_{\mathrm{L}}} = \frac{2\sqrt{2}}{3\sqrt{3}} \frac{H_{\mathrm{cth}}}{\lambda_{\mathrm{L}}} = 0.544 \frac{H_{\mathrm{cth}}}{\lambda_{\mathrm{L}}}$$

Pb:
$B_{\mathrm{cth}} \approx 80$ mT, $\lambda_{\mathrm{L}} \approx 40$ nm
$\Rightarrow\ J_c^{\mathrm{GL}} \approx 8 \times 10^{11}$ A/m²

Nb:
$B_{\mathrm{cth}} \approx 200$ mT, $\lambda_{\mathrm{L}} \approx 40$ nm
$\Rightarrow\ J_c^{\mathrm{GL}} \approx 2 \times 10^{12}$ A/m²

- note: according London theory we would expect $J_c^{\mathrm{GL}} = H_{\mathrm{cth}}/\lambda_{\mathrm{L}}$
  (London theory does not take into account reduction of OP with increasing J_s)

6.2.1 Depairing Critical Current Density

- Gedanken experiment: what is the critical current of a Pb (type-I SC) rod with large diameter d ?

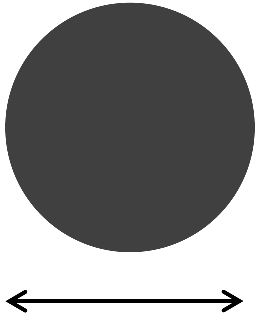

$d = 1\text{cm}$

critical current $I_c = J_c^{\mathrm{GL}} \cdot A = J_c^{\mathrm{GL}} \cdot \pi \left(\frac{d}{2}\right)^2 \approx 6 \times 10^7$ A ????

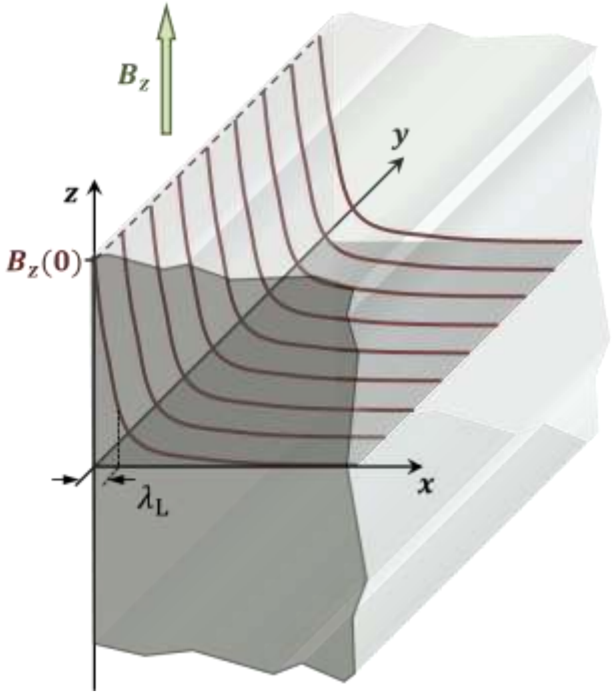

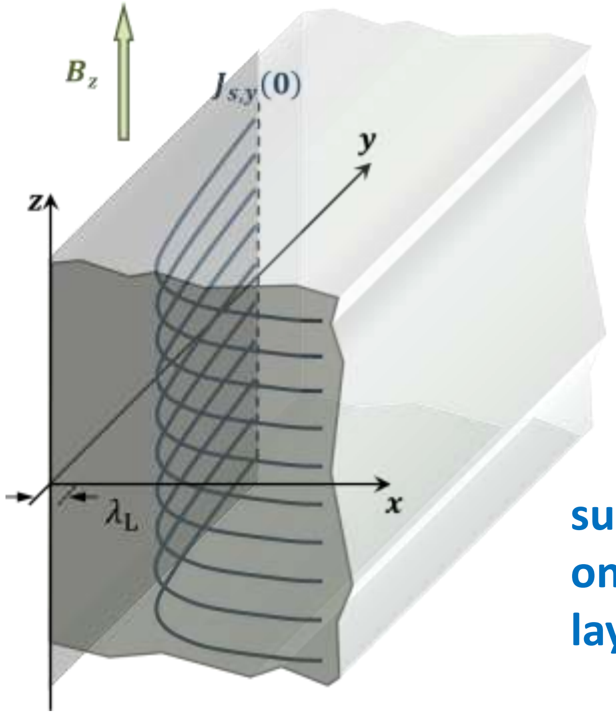

supercurrent flows only in thin surface layer of thickness λ_L

London theory (cf. 3.1.1): $B_z(x) = B_z(0)\ \exp\left(-\frac{x}{\lambda_L}\right)$ $J_{s,y}(x) = J_{s,y}(0)\exp\left(-\frac{x}{\lambda_L}\right)$

6.2.1 Depairing Critical Current Density

- supercurrent in a type-I superconductor flows only within surface layer of thickness λ_L

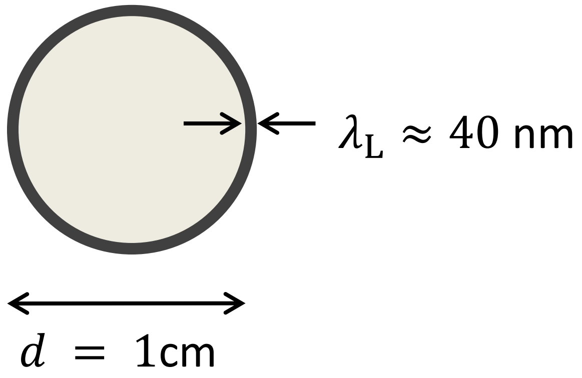

critical current: $I_c = J_c^{\mathrm{GL}} \cdot A = J_c^{\mathrm{GL}} \cdot \pi d \lambda_\mathrm{L} \approx 1 \times 10^3$ A

technical critical current density:

$$J_c^{\mathrm{tech}} = \frac{I_c}{\pi (d/2)^2} \approx 10 \text{ A/mm}^2$$

comparable to Cu-wire

- possible solutions:
  - use multifilament wire with $d < \lambda_\mathrm{L}$ → difficult to fabricate
  - use **type-II superconductor**

supercurrent flow in mixed state is not limited to thin surface layer

Summary of Lecture No. 11

power applications of superconductors require high T_c, B_{c2}, J_c

– examples: power transmission lines, fault current limiters, NMR/MRI magnets, magnets for fusion, magnetic levitation, high magnetic fields for research, ….

materials requirements

– high supercurrent densities at high operation temperatures and high magnetic fields
– only type-II superconductors are relevant
– simple and cheap manufacturing, abundant chemical elements

depairing critical current density

– **kinetic energy = binding energy of Cooper pairs**
– Calculation by GL theory for 1D conductor: $J_c^{\mathrm{GL}} = 0.544 \frac{H_{\mathrm{cth}}}{\lambda_{\mathrm{L}}}$:

depinning critical current density

– **Lorentz force on flux lines = pinning force due to pinning potential**
– high depinning critical current densities require defect engineering: large density, ideal size, columnar structure, …
– collective pinning: interaction of elastic flux line lattice with disordered pinning potential

Superconductivity and Low Temperature Physics I

Lecture No. 12

R. Gross

6 Flux Pinning and Critical Currents

type-II superconductors:

$$\kappa = \lambda_{\mathrm{GL}}/\xi_{\mathrm{GL}} \leq 1/\sqrt{2} \quad \text{type I superconductor}$$
$$\kappa = \lambda_{\mathrm{GL}}/\xi_{\mathrm{GL}} \geq 1/\sqrt{2} \quad \text{type II superconductor}$$

- partial field penetration above B_{c1}
  → $B_i > 0$ for $B_{\mathrm{ext}} > B_{c1}$
  → ***Shubnikov phase*** between $B_{c1} \leq B_{\mathrm{ext}} \leq B_{c2}$
  → ***upper and lower critical fields*** B_{c1} ***and*** B_{c2}

- in mixed state field penetrates the superconductor

→ ***current flow is not restricted to thin surface layer***

→ ***high values of*** B_{c2}

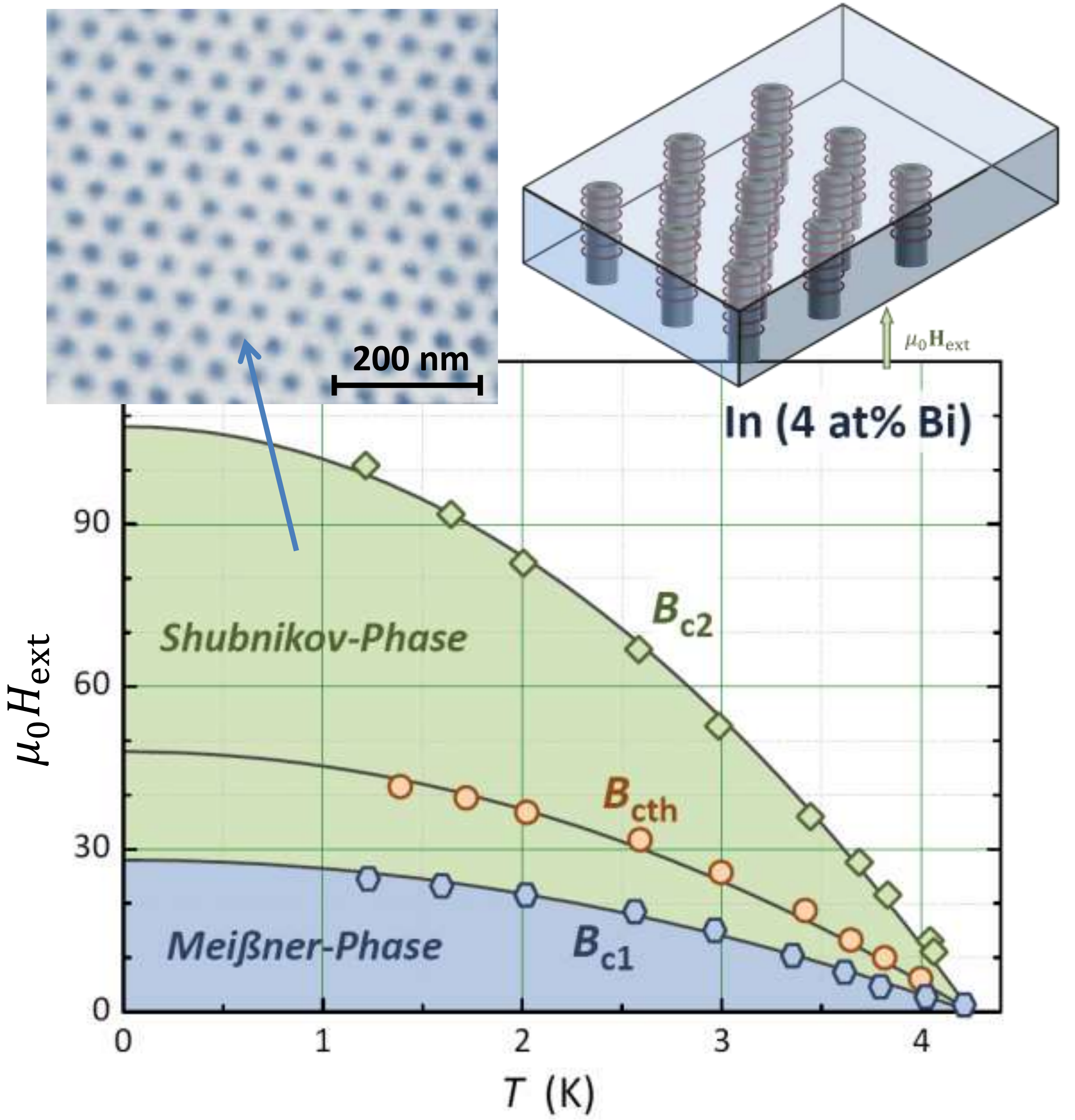

6.2.2 Depinning Critical Current Density

extreme type-II superconductors ($\kappa >> 1$) have very high B_{c2} → high field operation

B_{cth} and λ_{L} of type-I superconductors

Element	Al	In	Nb	Pb	Sn	Ta	Tl	V
T_c [K]	1.19	3.408	9.25	7.196	3.722	4.47	2.38	5.46
B_{cth} [mT]	10.49	28.15	206	80.34	30.55	82.9	17.65	140
$\lambda_{\mathrm{L}}(0)$ [nm]	50	65	32-45	40	50	35		40
κ_∞	0.03	0.06	~ 0.8	0.4	0.1	0.35	0.3	0.85

B_{c2} and λ_{L} of type-II superconductors

Verbindung	NbTi	Nb_3Sn	NbN	PbIn (2-30%)	PbIn (2-50%)	Nb_3Ge	V_3Si	$YBa_2Cu_3O_7$ (*ab*-Ebene)
T_c [K]	$\simeq 10$	$\simeq 18$	$\simeq 16$	$\simeq 7$	$\simeq 8.3$	23	16	92
B_{c2} [T]	$\simeq 10.5$	$\simeq 23$–29	$\simeq 15$	$\simeq 0.1$–0.4	$\simeq 0.1$–0.2	38	20	160 ± 25
$\lambda_{\mathrm{L}}(0)$ [nm]	$\simeq 300$	$\simeq 80$	$\simeq 200$	$\simeq 150$	$\simeq 200$	90	60	$\simeq 140 \pm 10$
κ_∞	$\simeq 75$	$\simeq 20$–25	$\simeq 40$	$\simeq 5$–15	$\simeq 8$–16	30	20	$\simeq 100 \pm 20$

6.2.2 Depinning Critical Current Density

superconducting transport current in the mixed state of a type-II superconductor

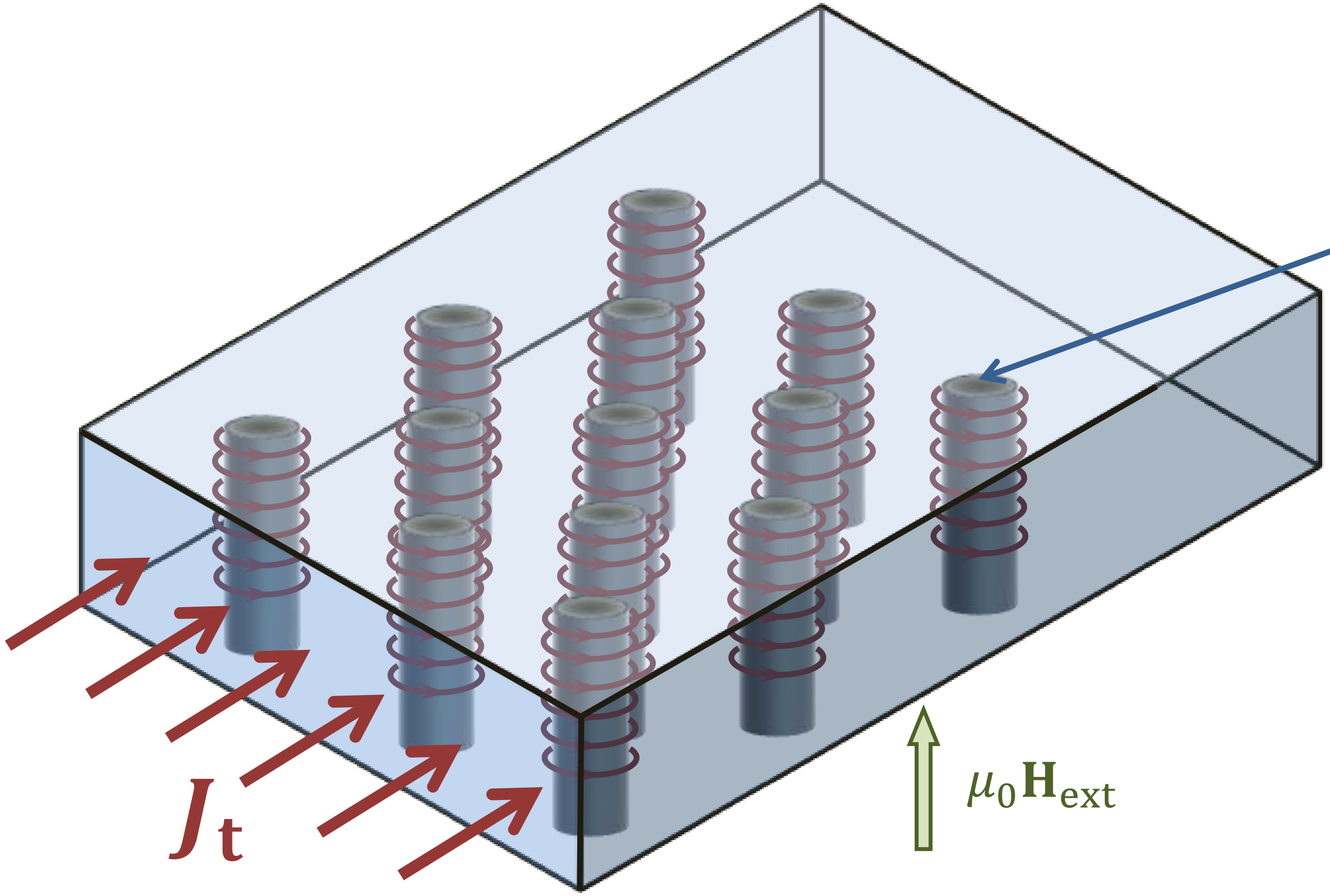

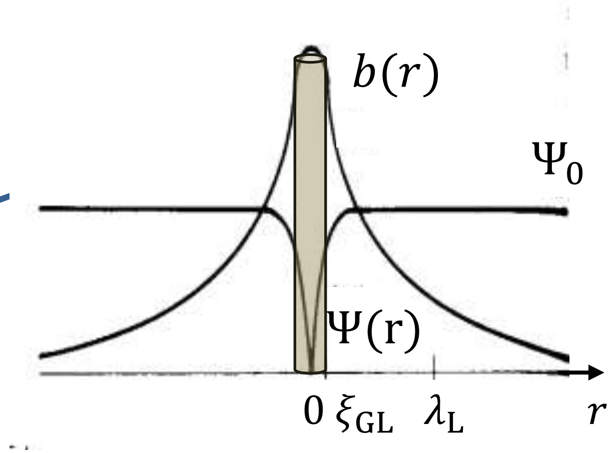

cross-sectional view of flux line

$$J_s(r) \propto \partial b(r)/\partial r$$

- *how does the transport current J_t interact with the vortex lattice and the associated circulating supercurrents ??*

6.2.2 Depinning Critical Current Density

interaction of a transport current with the vortex lattice:

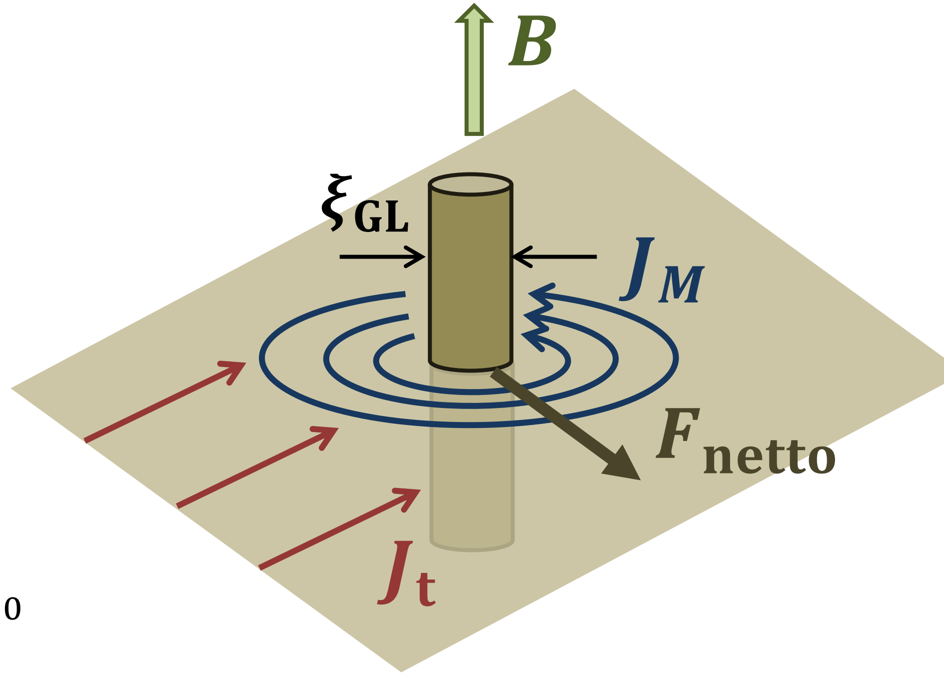

- Lorentz force on single flux line: $\mathbf{F}_{\rm L} = L \int_A \mathbf{J}_{\rm t} \times \mathbf{b} \; \mathrm{d}A$
- with homogeneous $\mathbf{J}_{\rm t}$: $\mathbf{F}_{\rm L} = L\mathbf{J}_{\rm t} \times \underbrace{\int_A \mathbf{b} \; \mathrm{d}A}_{} = L\mathbf{J}_{\rm t} \times \widehat{\Phi}_0$

  $\widehat{\Phi}_0 =$ vector of length Φ_0 and direction of $\mathbf{B}$

- in mixed state of type-II SC: many flux lines with areal density n_Φ resulting in average flux density $\mathbf{b} = n_\Phi \widehat{\Phi}_0$:

$$\boxed{\mathbf{f}_{\rm L} = \frac{\mathbf{F}_{\rm L}}{L} n_\Phi = \mathbf{J}_{\rm t} \times n_\Phi \widehat{\Phi}_0 = \mathbf{J}_{\rm t} \times \mathbf{b}}$$

average Lorentz force per volume

$\mathbf{f}_{\rm L}$ results in force on charge carriers of transport current, which cannot leave conductor

➔ ***force on flux lines (actio = reactio) leads to flux motion perpendicular to applied transport current***

6.2.2 Depinning Critical Current Density

origin of force acting on a flux line (plausibility check)

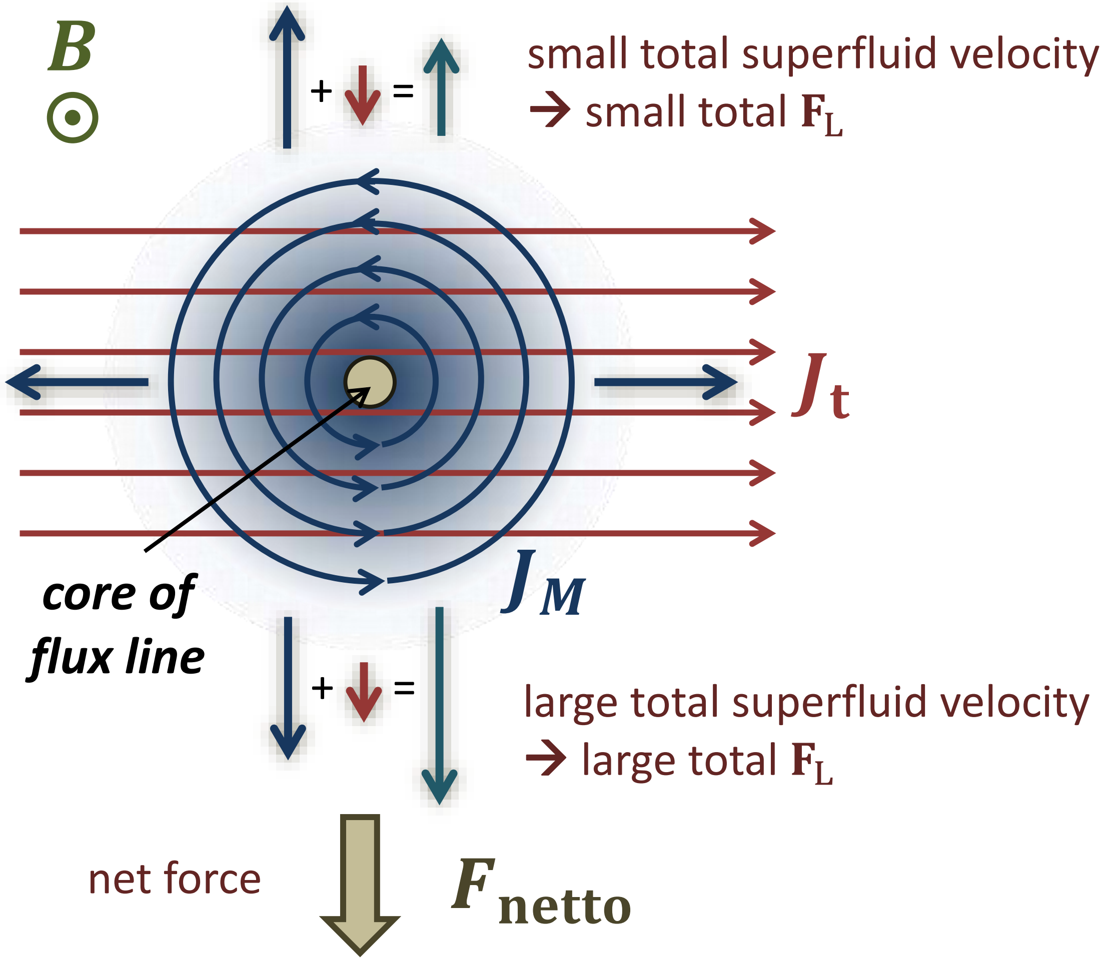

- without transport current: zero net force
- *contributions of circulating current cancel*

analogy to Magnus force

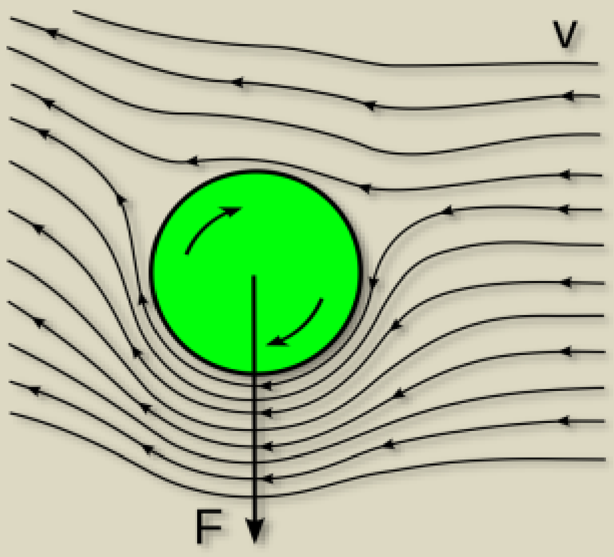

- ***Bernoulli's principle***: an increase in the speed of the fluid occurs simultaneously with a decrease in pressure or a decrease in the fluid's potential energy

6.2.2 Depinning Critical Current Density

Lorentz force on single flux line

- Lorentz force on single flux line: $\mathbf{F}_\mathrm{L} = L \int_A \mathbf{J}_\mathrm{t} \times \mathbf{b}\; \mathrm{d}A$

homogeneous

$$\mathbf{F}_\mathrm{L} = L\mathbf{J}_\mathrm{t} \times \underbrace{\int_A \mathbf{b}\; \mathrm{d}A}_{\widehat{\Phi}_0} = L\mathbf{J}_\mathrm{t} \times \widehat{\Phi}_0$$

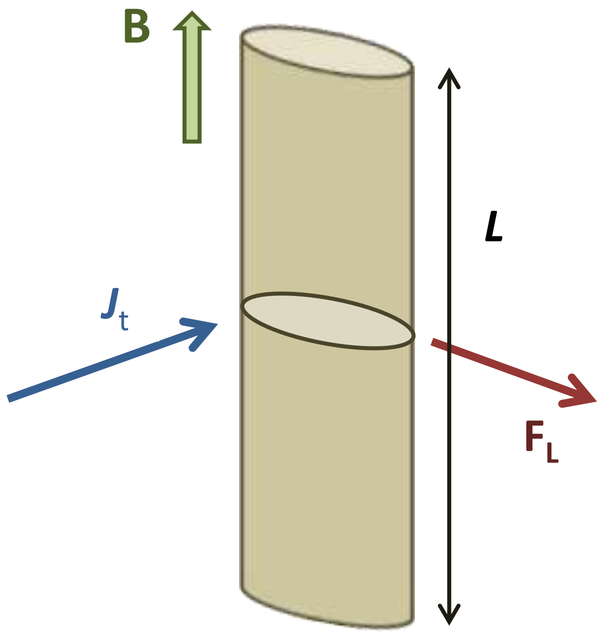

- force per unit length of flux line: $\boxed{\dfrac{\mathbf{F}_\mathrm{L}}{L} = \mathbf{J}_\mathrm{t} \times \widehat{\Phi}_0}$

- $\mathbf{F}_\mathrm{L}$ causes motion of the flux line
  - what is the **velocity v_L** of the flux line (depends on damping)
  - what is the **work done by the Lorentz force**

6.2.2 Depinning Critical Current Density

flux line motion

$$\oint_{\partial A} (\mathbf{E} + \mathbf{u} \times \mathbf{B}) \cdot \mathrm{d}\mathbf{s} = -\frac{\mathrm{d}}{\mathrm{dt}} \int_A \mathbf{B} \cdot \hat{\mathbf{n}} \, \mathrm{d}A$$

- ***Faraday's law of induction***:
  the induced electromotive force (EMF) in any closed circuit is equal to the time rate of change of the magnetic flux through the circuit.

- ***electromotive force*** (EMF):

$$\mathrm{EMF} = \frac{1}{e} \oint_{\partial A} \mathbf{F} \cdot \mathrm{d}\mathbf{s} = \frac{1}{e} \oint_{\partial A} (e\mathbf{E} + e\mathbf{v}_{\mathrm{L}} \times \mathbf{B}) \cdot \mathrm{d}\mathbf{s} = \underbrace{-\frac{\mathrm{d}}{\mathrm{dt}} \int_A \mathbf{B} \cdot \hat{\mathbf{n}} \, \mathrm{d}A}_{=\mathbf{0}}$$

⇨ $\mathrm{EMF} = \mathbf{0}$ **no flux change**

⇨ $\mathbf{E} = -\mathbf{v}_{\mathrm{L}} \times \mathbf{B}$ **electric field || transport current**

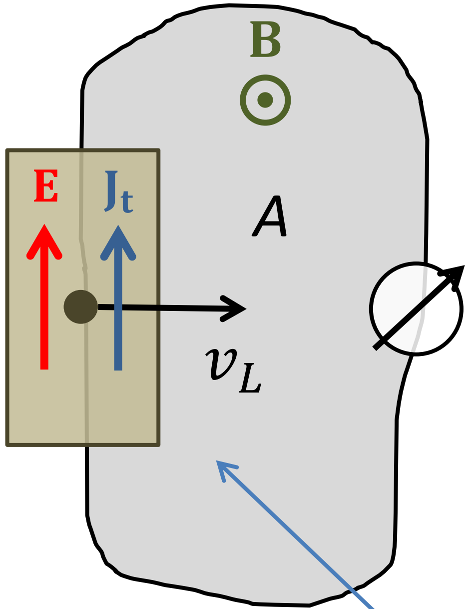

flux density inside loop does not change

- ***dissipation by moving flux line:***
  - motion with velocity $\mathbf{v}_{\mathrm{L}}$ induces electric field $\mathbf{E} = -\mathbf{v}_{\mathrm{L}} \times \mathbf{B} = \mathbf{B} \times \mathbf{v}_{\mathrm{L}}$
  - $\mathbf{E}$ is parallel to $\mathbf{J}_{\mathrm{t}}$ → acts like **"resistive" electric field**

6.2.2 Depinning Critical Current Density

flux line motion – other point of view: power balance

- generated power for - single flux line: $P_1 = \mathbf{F}_\mathrm{L} \cdot \mathbf{v}_\mathrm{L}$
  - N flux lines: $P_N = N\, \mathbf{F}_\mathrm{L} \cdot \mathbf{v}_\mathrm{L}$

- power balance: $P_N = N\, \mathbf{F}_\mathrm{L} \cdot \mathbf{v}_\mathrm{L} = V\, I_\mathrm{t}$

voltage drop along sample

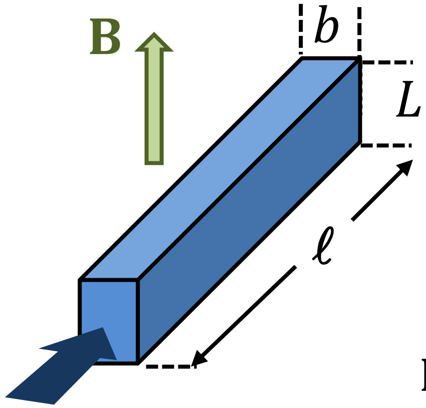

$$\mathbf{F}_\mathrm{L} = L \mathbf{J}_\mathrm{t} \times \widehat{\Phi}_0$$

$$\mathbf{E} = \frac{V}{\ell} = \frac{N\, \mathbf{F}_\mathrm{L} \cdot \mathbf{v}_\mathrm{L}}{I_\mathrm{t}\ \ell}\, \hat{\mathbf{J}}_\mathrm{t} = \frac{NL\, (\mathbf{J}_\mathrm{t} \times \widehat{\Phi}_0) \cdot \mathbf{v}_\mathrm{L}}{J_\mathrm{t} bL\ \ell}\, \hat{\mathbf{J}}_\mathrm{t} = \frac{N(\hat{\mathbf{J}}_\mathrm{t} \times \widehat{\Phi}_0) \cdot \mathbf{v}_\mathrm{L}}{b\ell}\, \hat{\mathbf{J}}_\mathrm{t} = \left[(\hat{\mathbf{J}}_\mathrm{t} \times \mathbf{B}) \cdot \mathbf{v}_\mathrm{L}\right]\, \hat{\mathbf{J}}_\mathrm{t}$$

sample length ℓ

sample cross-section bL perpendicular to $\mathbf{J}_\mathrm{t}$

cross-sectional area $b\ell$ perpendicular to $\mathbf{B}$

$\mathbf{E} \,||\, \hat{\mathbf{J}}_\mathrm{t}$ ➔ superconductor shows resistive behavior: ***flux-flow resistance***

6.2.2 Depinning Critical Current Density

phase change due to flux motion:

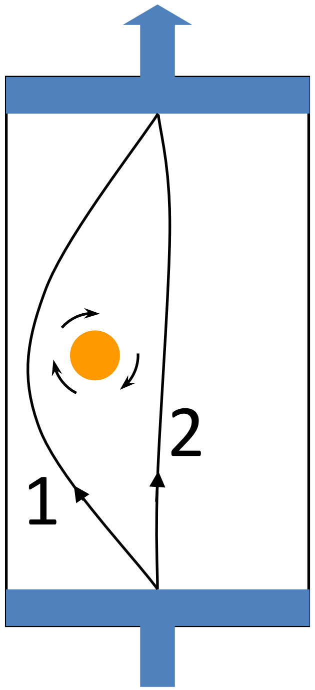

- assumption: single flux line in sample
- phase difference between the sample ends:

$$\delta\theta_1 = \int_{\text{path 1}} \nabla\theta \, \mathrm{d}s$$

- integration path 2:

$$\delta\theta_2 = \int_{\text{path 2}} \nabla\theta \, \mathrm{d}s = \underbrace{\int_{\text{path 2}} \nabla\theta \, \mathrm{d}s - \int_{\text{path 1}} \nabla\theta \, \mathrm{d}s}_{\oint \nabla\theta \, \mathrm{d}s} + \int_{\text{path 1}} \nabla\theta \, \mathrm{d}s = \underbrace{\oint \nabla\theta \, \mathrm{d}s}_{2\pi} + \delta\theta_1 = 2\pi + \delta\theta_1$$

- note: only the phase factor $\mathrm{e}^{\imath\theta}$ must be unambiguous

6.2.2 Depinning Critical Current Density

moving flux line:

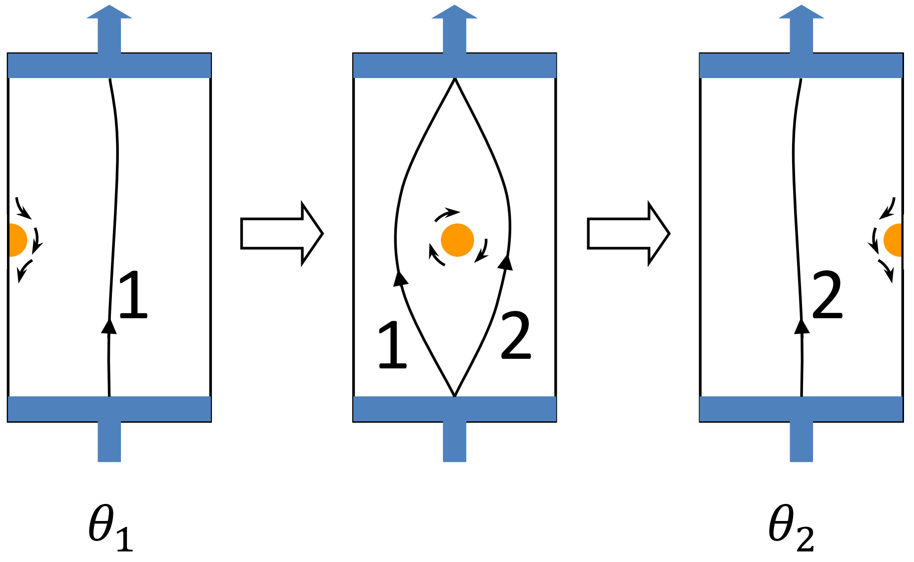

- crossing of single flux line changes phase difference by $\varphi = \theta_2 - \theta_1 = 2\pi$

- required time for crossing: $\delta t = b/v_\mathrm{L}$

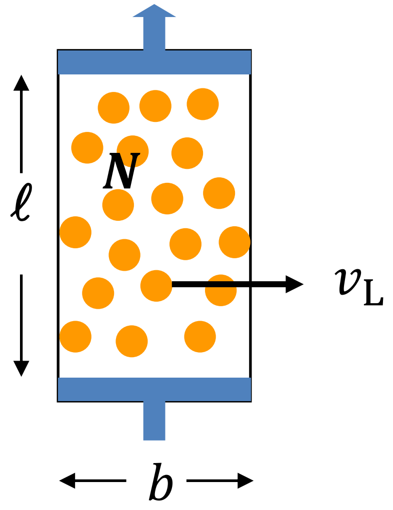

$$\frac{\partial \varphi}{\partial t} = N\frac{2\pi}{\delta t} = N\frac{2\pi}{b/v_\mathrm{L}} = \frac{\Phi}{\Phi_0}\frac{2\pi}{b}v_\mathrm{L} = \frac{B\;b\ell}{\Phi_0}\frac{2\pi}{b}v_\mathrm{L} = Bv_\mathrm{L}\,\ell\,\frac{2\pi}{\Phi_0}$$

temporal change of phase difference due to motion of flux lines

6.2.2 Depinning Critical Current Density

relation between temporal change of phase difference $\partial\varphi/\partial t$ and electric field $\mathbf{E}$

$$\frac{\partial\varphi}{\partial t} = B v_{\mathrm{L}}\,\ell\,\frac{2\pi}{\Phi_0} = B v_{\mathrm{L}}\,\ell\,\frac{2e}{\hbar}$$

- we make use of $\mathbf{E} = -\mathbf{v}_{\mathrm{L}} \times \mathbf{B} = \mathbf{B} \times \mathbf{v}_{\mathrm{L}} \quad \Rightarrow \quad |\mathbf{E}| = B\, v_{\mathrm{L}}$

$$\boxed{\frac{\partial\varphi}{\partial t} = \frac{2e}{\hbar} B v_{\mathrm{L}}\,\ell = \frac{2e}{\hbar}\,E\ell = \frac{2eV}{\hbar}}$$

corresponds to 2nd Josephson Equation

6.2.2 Depinning Critical Current Density

power dissipation during vortex motion:

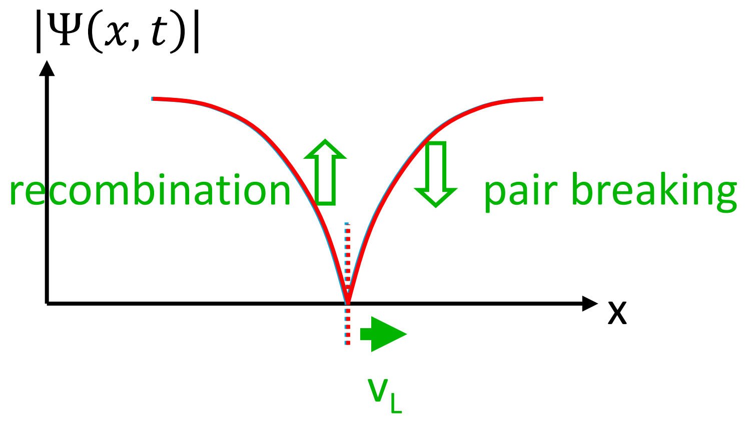

a. pair breaking and recombination:

- in front of flux-line: $|\Psi|$ decreases

  $\Rightarrow$ pairs have to break up

- pair breaking due to absorption of phonons:

- behind the flux-line: $|\Psi|$ increases

  $\Rightarrow$ recombination of pairs by phonon emission:

- finite phonon lifetime delays thermal equilibrium:

  irreversible process → friction, viscous flow

- electric energy is transferred to heat

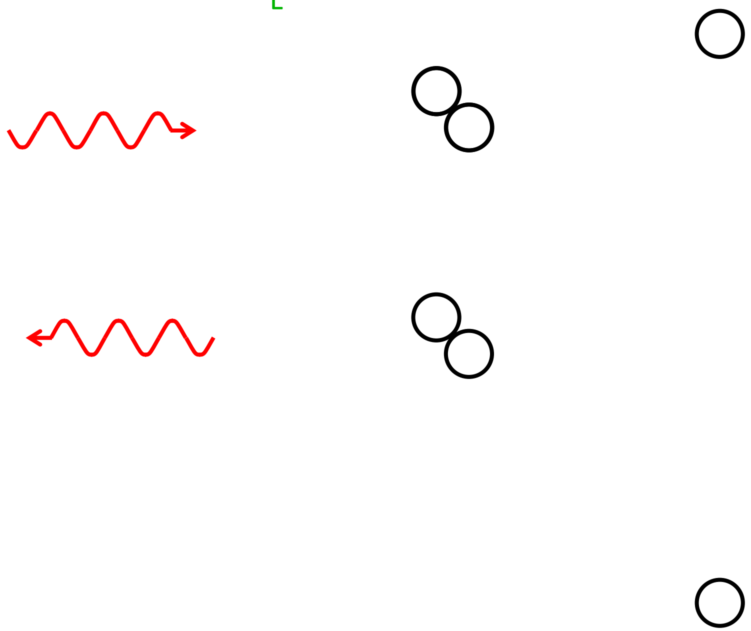

6.2.2 Depinning Critical Current Density

power dissipation during vortex motion:

b. eddy current losses:

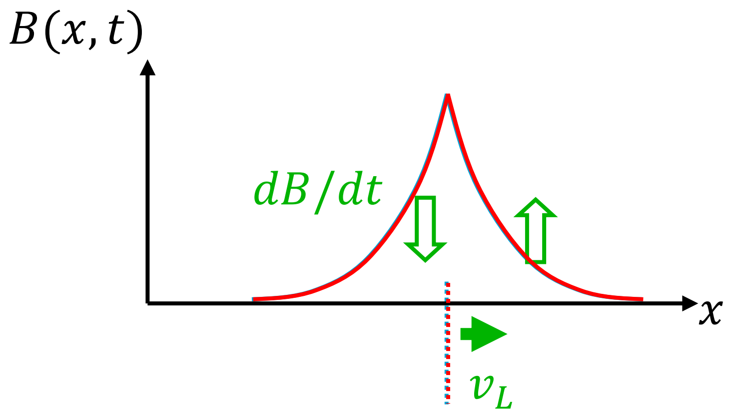

$$-\nabla \times \mathbf{E} = \frac{\partial B}{\partial t} = \frac{\partial B}{\partial x}\frac{\partial x}{\partial t} = \frac{\partial B}{\partial x} v_x$$

core of the flux line is considered as normal conductor

$\Rightarrow$ ***eddy current*** with ohmic losses

- ***both mechanisms lead to*** $E \propto v_L$ ➔ **viscous damping**
- balance between Lorentz and friction force: v_L becomes stationary

$$v_L \propto J_t \quad \Rightarrow \quad v_L \propto E$$

- we expect: $J_t \propto E$ ***Ohm's law → zero critical current density***

6.3 Flux Line Pinning

experimental result:

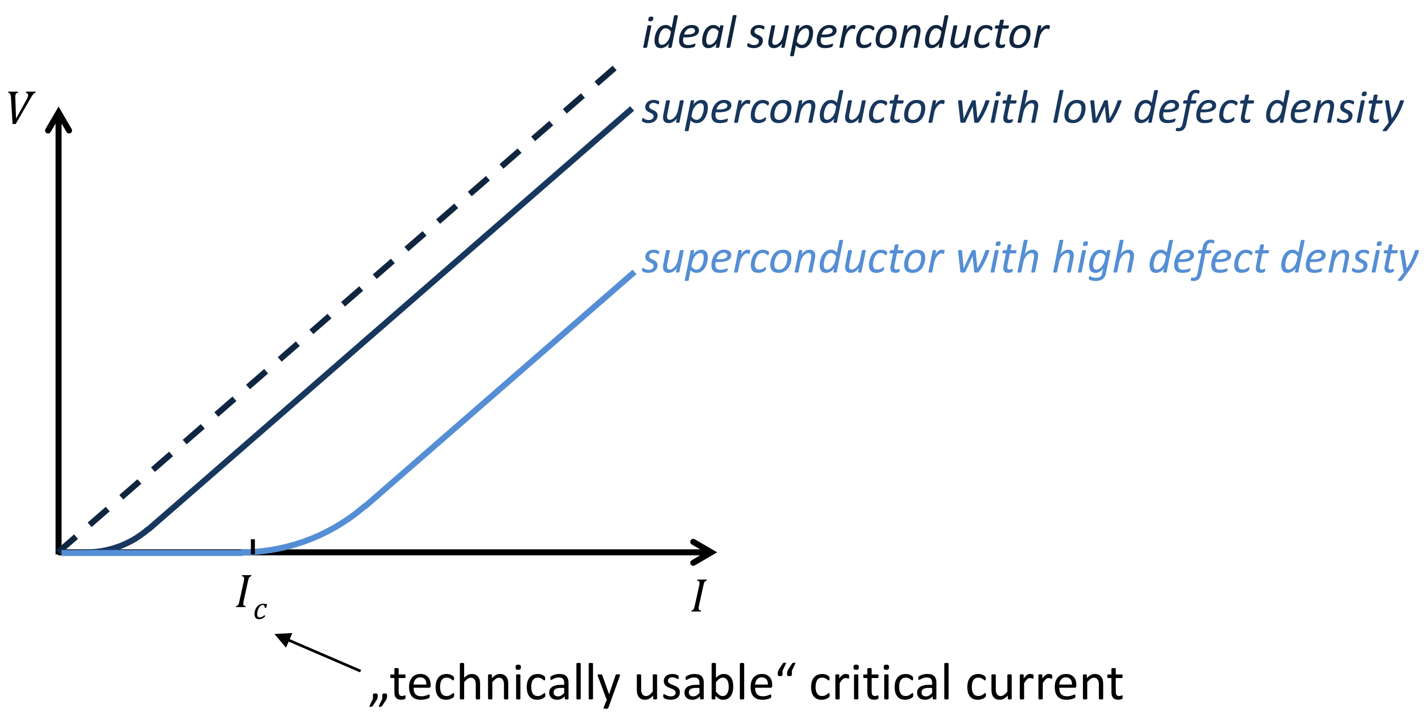

- I_c depends on defect density (and specific properties of defects)
- inhomogeneities pin flux-lines: ***flux line pinning***
- $v_L = 0$ is caused by flux pinning $\Rightarrow$ ***no work, no dissipation***

  $\Rightarrow$ ***no voltage drop***

pinning mechanism

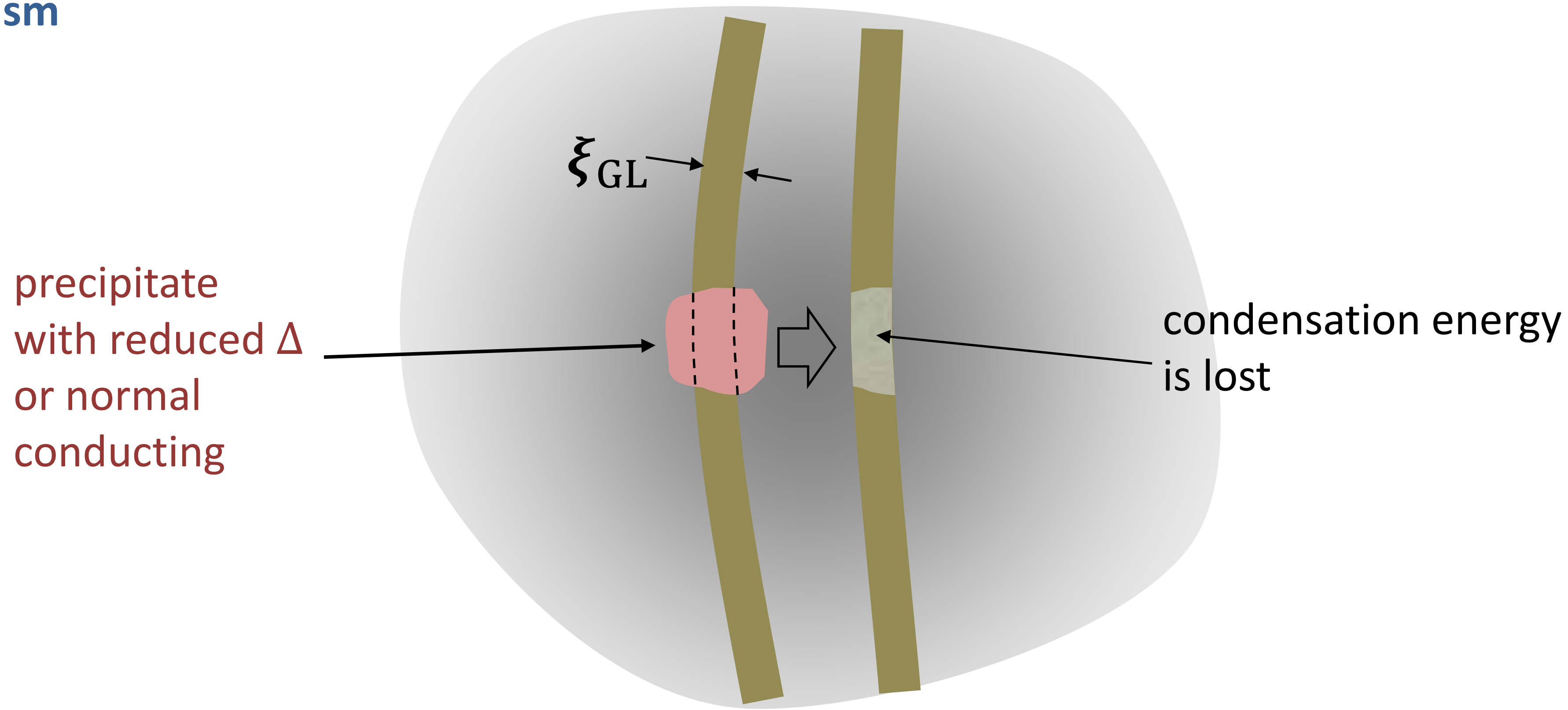

- at precipitate: normal vortex core causes no additional loss in condensation energy
- motion of vortex core from left to right position costs energy (condensation energy)
- effective binding forced at precipitate ➔ ***„pinning force"***
- most effective, if defect size $\approx \xi_{GL}$

6.3 Flux Line Pinning

pinning potential

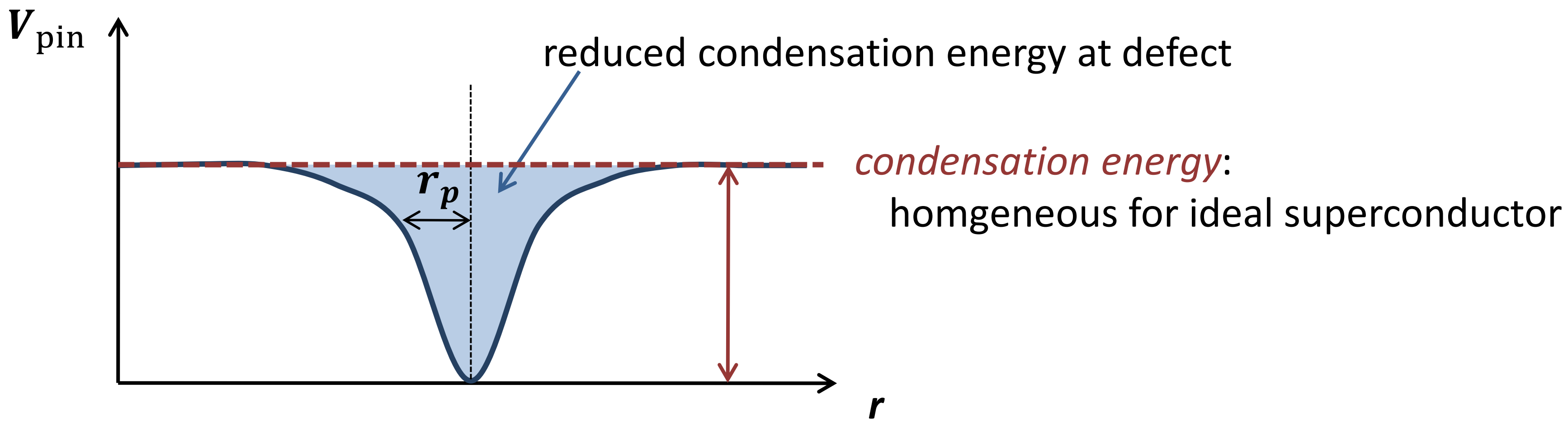

- pinning force: $F_\text{p} = -\frac{\partial V_p}{\partial r} \approx -\frac{E_\text{cond}}{r_p}$

→ reduce r_p to increase F_p
→ $E_\text{cond} = (E_\text{cond}/V)r_p^2 L \Rightarrow$ increase L (columnar defects)
→ optimum: $r_p \approx \xi_\text{GL}$ (vortex size ≈ pin size)

- for high-temperature superconductors: $\xi_\text{GL} \simeq 1$ nm and large condensation energy E_cond

→ very small pinning sites required
→ large pinning force

- problem for HTS: thermally activated escape of flux line → **thermally activated flux flow: TAFF**

$\frac{E_\text{cond}}{V}\,\xi_\text{GL}^3 \sim k_\text{B}T$ as ξ_GL small and operation T large

pinning of the flux line lattice

- **so far:** pinning of a single flux line
- **now:** pinning of the complete flux line lattice

→ complicated problem:
- flux line lattice is an elastic object
(stiffness of the lattice, flux lines can bend)
- pinning potential is usually highly disordered

- **example:** net pinning force of a completely stiff flux line lattice by statistical pinning potential vanishes
  - ➢ flux line lattice has to deform to adopt flux line positions to pinning potential
  - ➢ even if a single flux line does not sit in a potential well, it is pinned by the interaction with the other flux lines (rigidity of the lattice)

→ ***collective pinning theory***

see e.g.
Vortices in high-temperature superconductors
G. Blatter, M. V. Feigel'man, V. B. Geshkenbein, A. I. Larkin, and V. M. Vinokur
Rev. Mod. Phys. **66**, 1125 (1994)

6.3 Flux Line Pinning

pinning by surface roughness

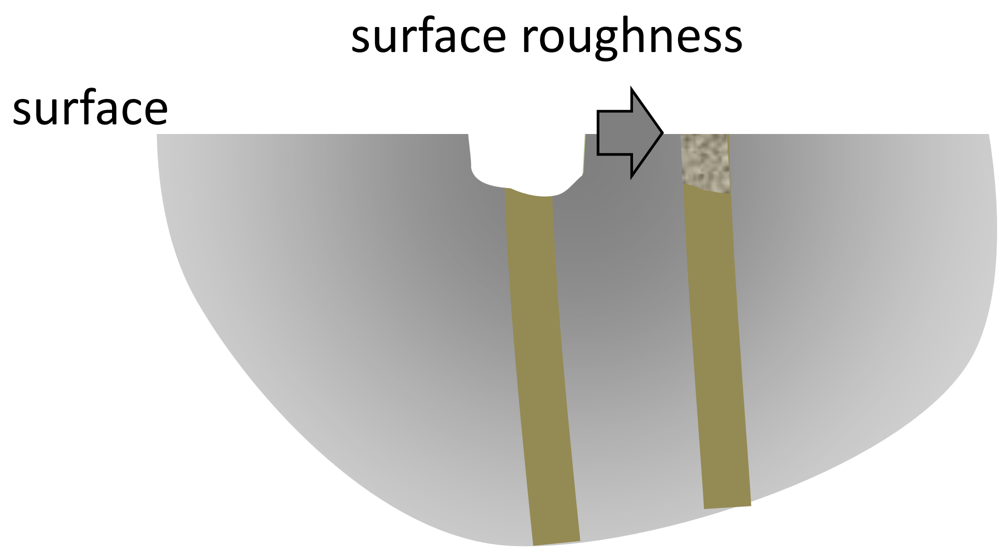

important for superconducting thin films

→ relative length difference of flux line at different positions may be large

6.3 Flux Line Pinning

J_c as a function of temperature and applied magnetic field:

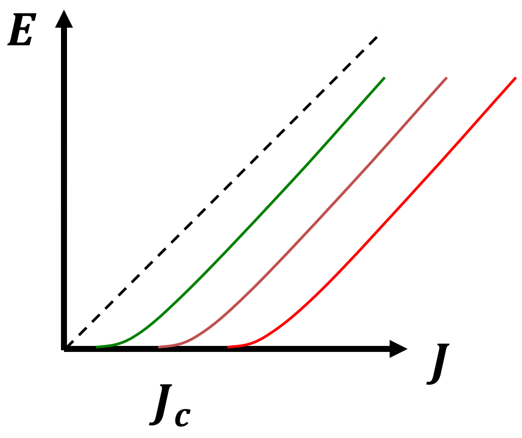

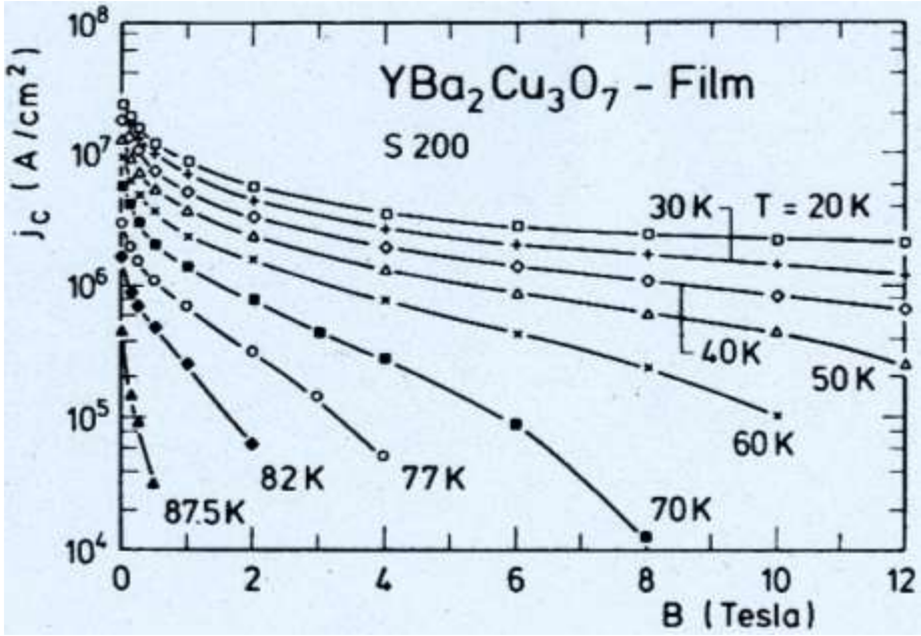

- decrease of J_c with increasing B: - several flux lines per pinning site, not enough pinning sites
- decrease of J_c with increasing T: - thermally activated flux motion
  - reduced condensation energy

6.4 Magnetization of Hard Superconductors

flux line pinning in an external field:

magnetization curve

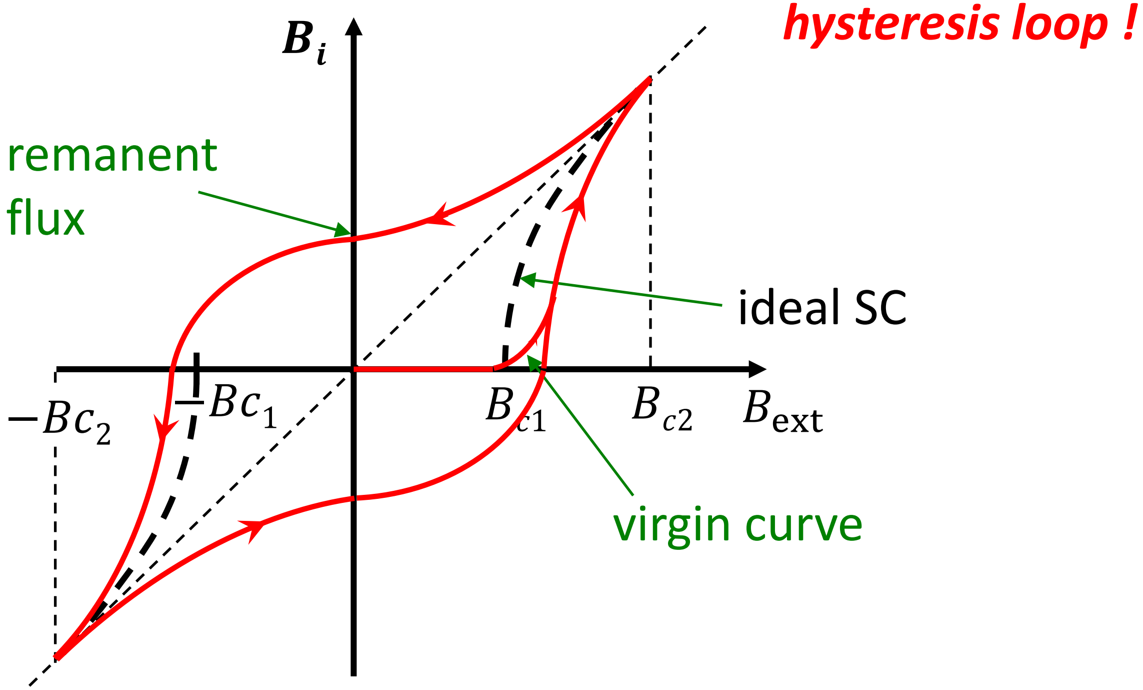

- B_{c1} and B_{c2} stay the same
- pinning prevents flux motion, i.e. penetration and exit of flux lines ➔ **hysteresis loop**
- B_i is inhomogeneous within the sample
- finite remanent flux density allows application of SC as permanent magnet
  for HTS: remanent flux density can exceed 15 T ➔ ***extremly strong permanent magnets***

magnetic flux distribution in sample:

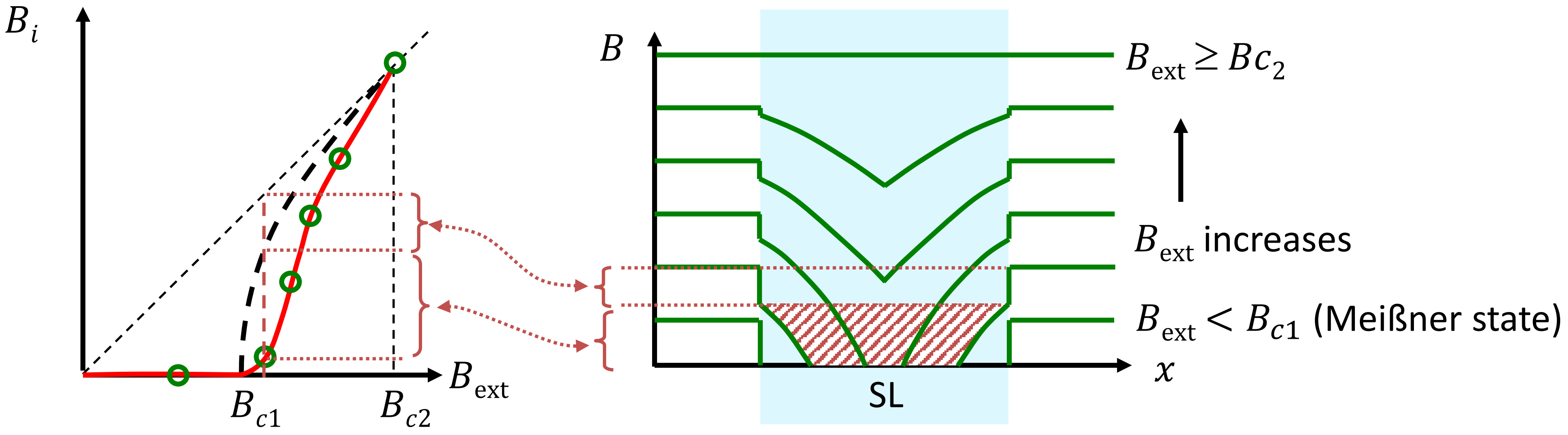

- sample surface: jump ↔ ideal magnetization curve
- within superconductor: gradient of flux density
- flux lines repel each other: motion if repulsion > pinning force
- gradient of flux density decreases with increasing magnetic field

6.4 Magnetization of Hard Superconductors

field distribution in sample (demagnetization):

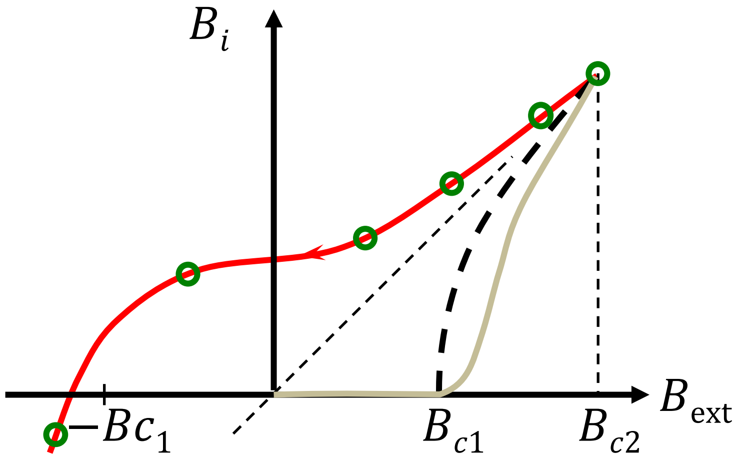

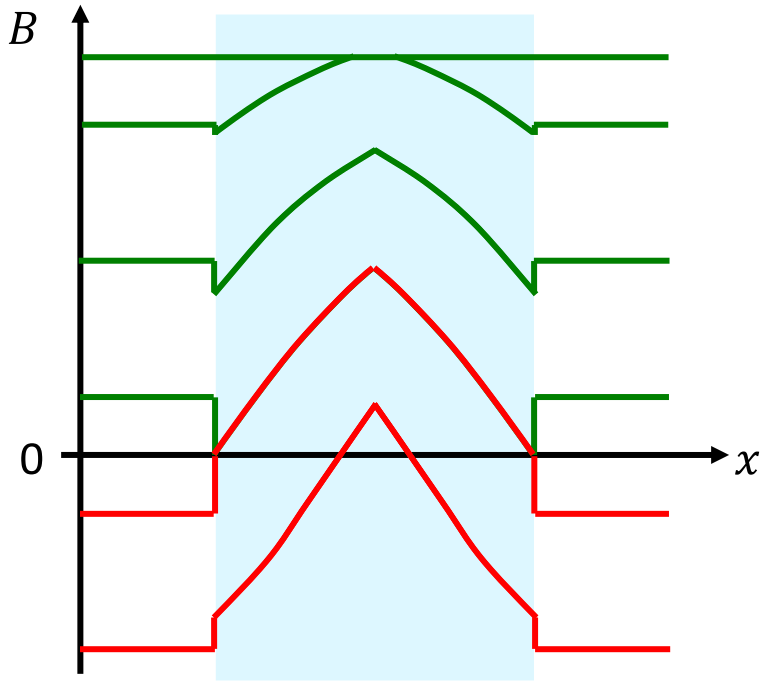

- gradient changes sign
- $B_{\text{ext}} < -Bc_1$: flux lines with opposite direction penetrate

recombination with frozen-in flux lines inside the superconductor

6.4 Magnetization of Hard Superconductors

Bean (critical state) model

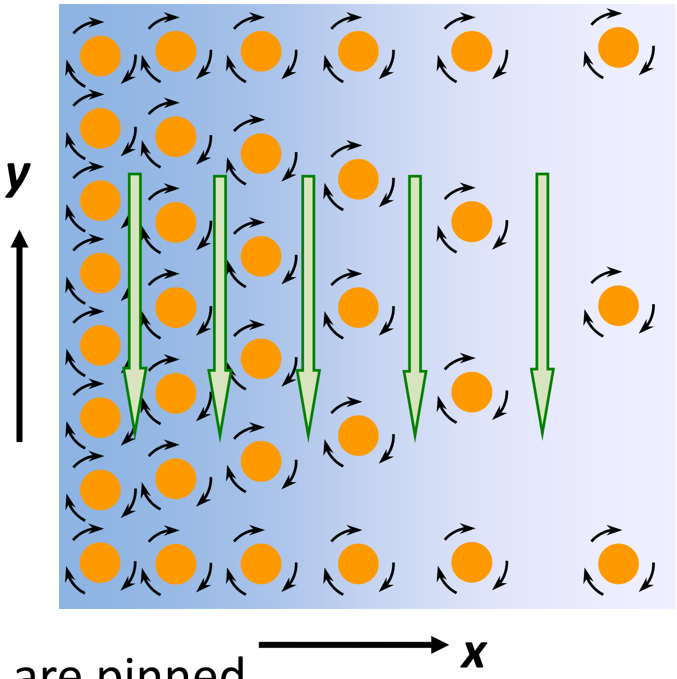

- flux gradient ↔ shielding current
- macroscopic average:

$$\nabla \times \mathbf{B}_i = \mu_0 \mathbf{J}_{\mathrm{scr}}$$

- here: $\dfrac{\partial B_{i,z}}{\partial x} = \mu_0 J_{\mathrm{scr},y}$
- for small $\partial B_{i,z}/\partial x$: $J_{\mathrm{scr}} < J_c \Rightarrow$ flux lines are pinned
- for large $\partial B_{i,z}/\partial x$: $J_{\mathrm{scr}} > J_c \Rightarrow$ flux lines move
- motion until $\boxed{J_{\mathrm{scr}} = J_c}$ *"critical state„* (similar critical slope of pile of sand)
- note:

  measurement of $\dfrac{\partial B_{i,z}}{\partial x} \Rightarrow J_c$

  J_c decreases with increasing $B_i \Rightarrow$ smaller slope

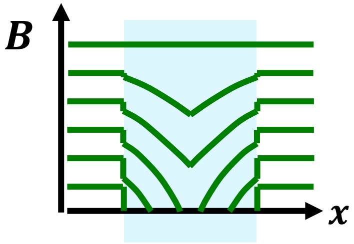

magneto-optical imaging of flux distribution

imaging technique: Faraday rotation $\propto \mathbf{B}_i(\mathbf{r})$

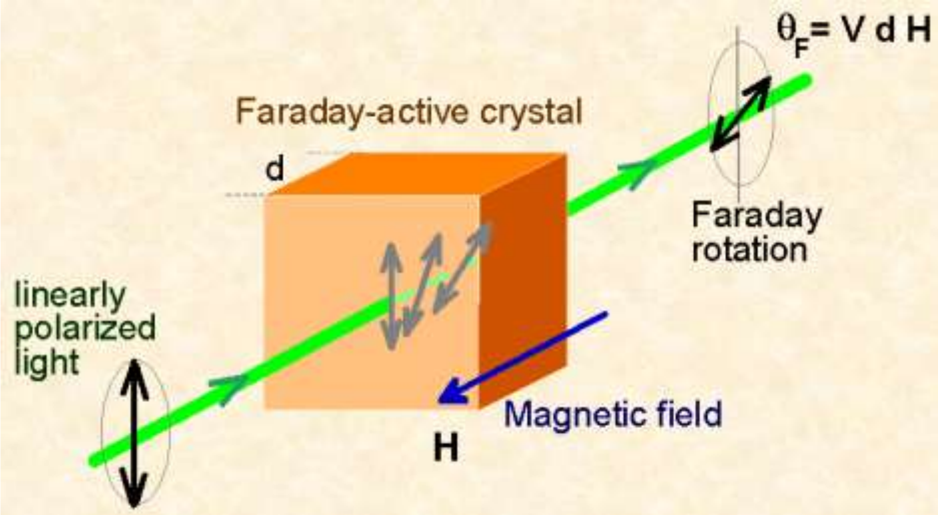

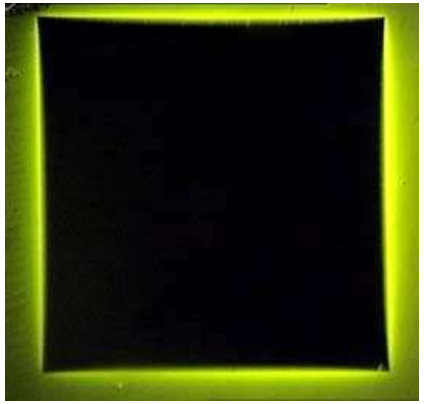

Meißner state

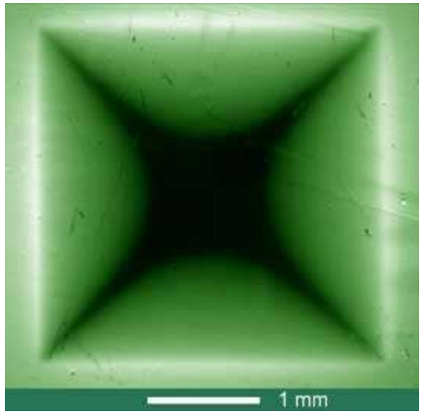

critical state

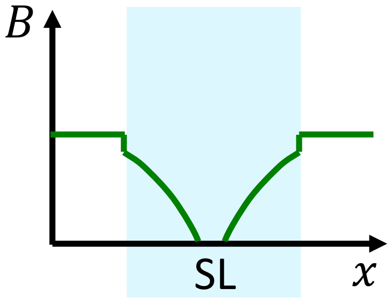

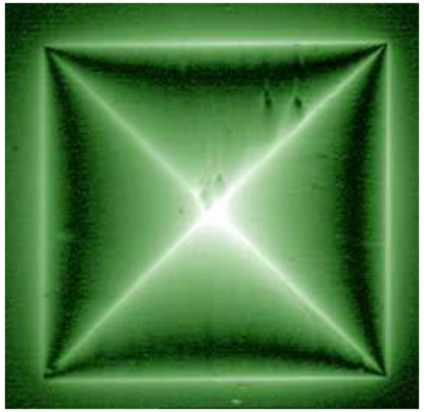

remanent state

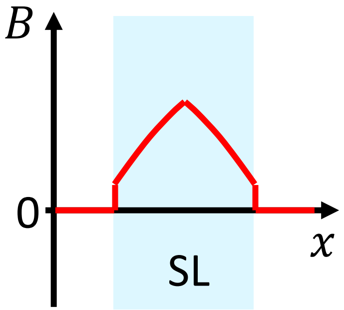

Summary of Lecture No. 12 (1)

depinning critical current density

- Lorentz force on flux lines = pinning force due to pinning potential
- high depinning critical current densities require defect engineering: large density, ideal size, columnar structure, …
- collective pinning: interaction of elastic flux line lattice with disordered pinning potential

flux line motion

- flux lines start to move if the Lorentz force exceeds the pinning force
- flux lines move perpendicular to current direction
- moving flux lines cause time change of phase difference and thereby a voltage drop $V \propto \dot{\varphi}$ in current direction ➔ no dissipationless current flow
- dissipationless supercurrent only if flux line motion is avoided by flux pinning
- engineering of pinning landscape: defects, surface roughness, ion bombardment, ...

critical state of superconductors

- flux pinning allows for finite gradient of the magnetic flux density
- maximum possible gradient determines depinning critical current density (Bean critical state model)
- flux pinning results in hysteretic magnetization curve with finite remanent flux density
  → application of superconductors as permanent magnets